Ore Geology Reviews xxx (2014) xxx–xxx

Contents lists available at ScienceDirect

Ore Geology Reviews

journal homepage: www.elsevier.com/locate/oregeorev

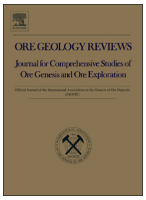

The Khopik porphyry copper prospect, Lut Block, Eastern Iran: Geology, alteration and mineralization, fluid inclusion, and oxygen isotope studies

A. Malekzadeh Shafaroudi [a,*], M.H. Karimpour [a], C.R. Stern [b]

[a] Research Center for Ore Deposits of Eastern Iran, Ferdowsi University of Mashhad, Iran
[b] Department of Geological Sciences, University of Colorado, CB-399, Boulder, CO 80309-399, USA

ARTICLE INFO

Article history:
Received 14 October 2012
Received in revised form 16 April 2014
Accepted 21 April 2014
Available online xxxx

Keywords:
Porphyry copper
Khopik
Lut Block
Alteration and mineralization
Microthermometry
Stable isotope

ABSTRACT

The Khopik porphyry copper (Au, Mo) prospect in Eastern Iran is associated with a succession of Middle to Late Eocene I-type, high-K, calc-alkaline to shoshonite, monzonitic to dioritic subvolcanic porphyry stocks emplaced within cogenetic volcanic rocks. Laser-ablation U-Pb zircon ages indicate that the monzonite stocks crystallized over a short time span during the Middle Eocene (39.0 ± 0.8 Ma to 38.2 ± 0.8 Ma) as result of subduction of the Afghan block beneath the Lut block.

Porphyry copper mineralization is hosted by the monzonitic intrusions and is associated with a hydrothermal alteration that includes potassic, sericitic-potassic, quartz-sericite-carbonate-pyrite (QSCP), quartz-carbonate-pyrite (QCP), and propylitic zones. Mineralization occurs as disseminated to stockwork styles, and as minor hydrothermal breccias. Some mineralization occurs in fault zones as quartz-sulfide veins telescoped onto the porphyry system. The main ore minerals are chalcopyrite and bornite with minorpyrite and magnetite and the highest Cu (0.01–0.9 wt.%), Au (>2 ppm), and Mo (<80 ppm) grades are closely associated with potassic alteration zones.

Unidirectional, pre-ore stage solidification texture (UST) represented by comb-quartz layers within the potassic alteration zone formed from a hypersaline brine (57–73 wt.% NaCl equiv.), low density vapor-rich fluids (4–22 wt.% NaCl equiv.) at temperatures of 482 °C to over 600 °C. The isotopic composition of oxygen ($\delta^{18}O_{water} = 8.7–8.9$ ‰) suggests that the quartz layers crystallized from magmatic-hydrothermal fluids that exsolved in the upper part of the monzonitic intrusions. Potassic alteration formed from high salinity fluids (51–73 wt.%) at temperatures between 432–592 °C, and low salinity vapor-rich solutions with 11–19 wt.% NaCl equiv. Later veinlets in the QSCP zone formed from lower salinity fluids (<47 wt.% NaCl equiv.) at temperatures between 332°–400 °C. The oxygen isotopic data for the early alteration zones ($\delta^{18}O_{water} = 9–9.3$ ‰ for potassic and 7.3 ‰ for QSCP) also indicate a magmatic origin for the ore fluids.

The widespread presence of Middle Eocene to Lower Oligocene magmatism and mineralization in Eastern Iran suggests the presence of another important porphyry copper belt in addition to the northwest-southeast Urumieh-Dokhtar copper belt of Iran.

1. Introduction

World-class porphyry copper deposits have long been recognized along the Middle to Late Miocene Urumieh-Dokhtar Magmatic Belt (UDMB) of Iran, are being mined (e.g., Sar Cheshmeh, Meiduk, and Sungun), and have been the subject of research studies for over forty years (Ahmadian et al., 2009; Berberian et al., 1982; Boomeri et al., 2009; Dimitrijevic, 1973; Forster, 1978; Ghasemi and Talbot, 2006; Hassanpour, 2010; Hooper et al., 1994; Jamali et al., 2010; Jankovic, 1984; Jung et al., 1976; Mohajjel et al., 2003; Shahabpour, 2005, 2007 Shafiei et al., 2009; Waterman and Hamilton, 1975). In contrast, little is known about the ore metal potential of other parts of Iran. The Karimpour (2007) established a database for a portion of eastern Iran, including Aster mineral mapping, aeromagnetic data, geology, petrologic model, as well as stream sediment geochemical data, and a number of prospects with potential for porphyry copper were identified (Khopik, Maherabad, Dehsalm, Chahshaljami, Shiekhabad, etc.).

The Khopik and Maherabad prospects were the subject of a PhD study by the first author (Malekzadeh Shafaroudi, 2009). In this paper we present the results of this study with an emphasis on the alteration and mineralization at the Khopik prospect. Fluid inclusion and oxygen isotopic data obtained for quartz crystals in UST layers and for selected

---

* Corresponding author at: Ferdowsi University of Mashhad, Research Center for Ore Deposit of Eastern Iran Mashhad, Khorasan Razavi province, Iran.
E-mail address: Shafaroudi@um.ac.ir (A. Malekzadeh Shafaroudi).

http://dx.doi.org/10.1016/j.oregeorev.2014.04.015
0169-1368/

Please cite this article as: Malekzadeh Shafaroudi, A., et al., The Khopik porphyry copper prospect, Lut Block, Eastern Iran: Geology, alteration and mineralization, fluid inclusion, and oxygen isotope studies, Ore Geol. Rev. (2014), http://dx.doi.org/10.1016/j.oregeorev.2014.04.015

alteration zones have been elaborated to assess the nature of the hydrothermal fluids responsible for alteration and mineralization.

2. Regional geology

The Khopik prospect is located in the Lut Block of Eastern Iran approximately 80 km SW of the town Birjand (Fig. 1). The Lut Block is one of several microcontinental blocks interpreted to have drifted from the northern margin of Gondwanaland during the Permian opening of the Neo-Tethys, which was subsequently accreted to the Eurasian continent in the Late Triassic during the closure of the Paleo-Tethys (Golonka, 2004). The tectonic and magmatic evolution of the Lut Block has been interpreted within an extensional setting (Jung et al., 1983; Samani and Ashtari, 1992; Tarkian et al., 1983). The presence of ophiolitic complexes in Eastern Iran between the Lut and the Afghan Blocks, led Saccani et al. (2010) to consider the subduction of the oceanic lithosphere at this zone. Eftekharnejad (1981) proposed that magmatism in the northern Lut area resulted from the subduction of Afghan Block beneath the Lut Block, and Berberian (1983) showed that igneous rocks at Lut Block had a calc-alkaline arc signature. The accretionary prism-fore arc basin polarity, the structural vergence and younging of the accretionary prism to the southwest are consistent with a northeast-dipping subduction scenario (Tirrul et al., 1983). Recently, asymmetric subduction models have been discussed for situations similar to that of the Lut Block (Arjmandzadeh et al., 2011; Doglioni et al., 2009).

The Lut Block extends some 900 km from the Doruneh Fault in the north to the Jaz-Morian basin in the south and is ~ 200 km wide (Stocklin and Nabavi, 1973). The Lut Block consists of a pre-Jurassic metamorphic basement, Jurassic sedimentary rocks and several generations of Late Mesozoic and Cenozoic intrusive and/or volcanic rocks (Camp and Griffis, 1982; Tirrul et al., 1983). Radiometric age data indicate that the oldest magmatic activity in the central Lut Block took place in the Jurassic (Tarkian et al., 1983). Rb-Sr isotope data from the whole-rock and the biotite from the Sorkh Kuh granitoid yield Middle to Late Jurassic ages (164.8 ± 1.9 Ma and 170 ± 1.9 Ma, respectively; Tarkian et al., 1983). Intrusive rocks of a similar age are also recognized in the Deh-Salm metamorphic complex in the eastern Lut Block (Mahmoudi et al., 2010). Further to the north, magmatic activity started in Upper Cretaceous (75 Ma) and generated both volcanic and intrusive rocks (Tarkian et al., 1983). The Middle Eocene (47 Ma) was characterized by alkaline and shoshonitic volcanism with a peak at the end of the Eocene. In addition, calc-alkaline basalts and basaltic andesites erupted in the Eocene-Oligocene (40–31 Ma) (Tarkian et al., 1983).

Several sulfide deposits are known from Eastern Iran, in the vicinity of the Khopik prospect, including the Maherabad porphyry-type Cu-Au,

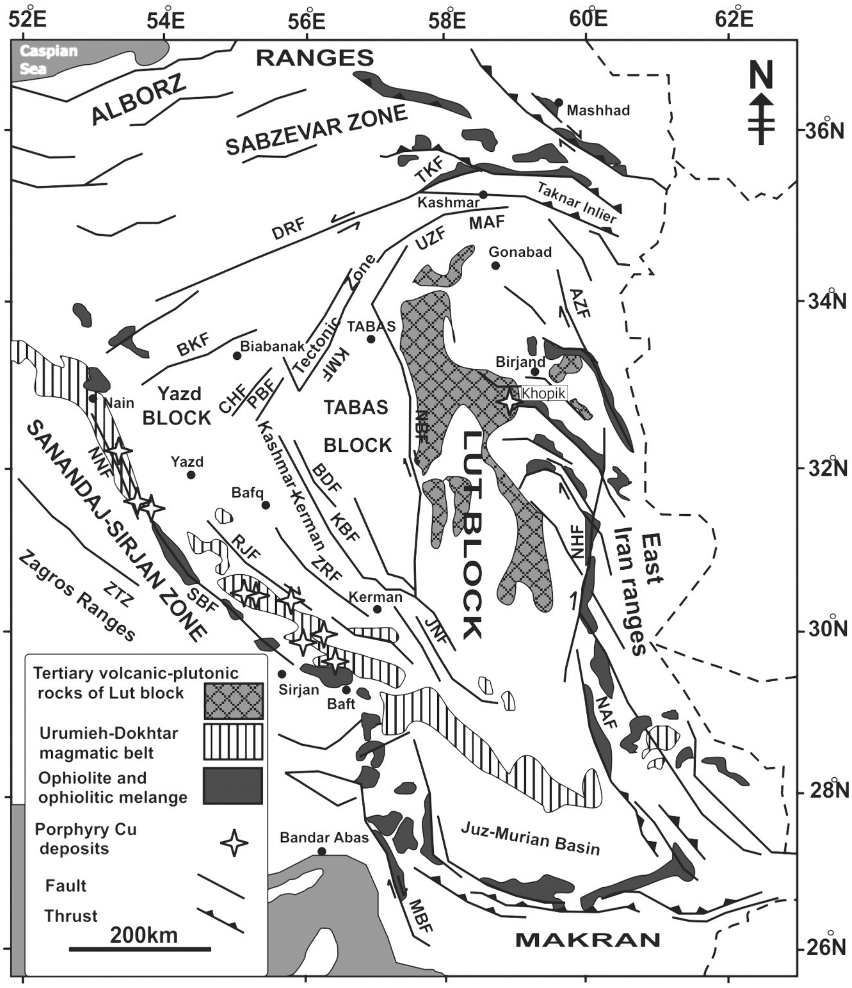

Fig. 1. The structural map of Central-East Iran and its crustal blocks (compiled and modified from Alavi, 1991; Berberian, 1981; Haghipour and Aghanabati, 1989; Jackson and McKenzie, 1984; Lindenberg et al., 1984). AZF = Abiz Fault; BDF = Behabad Fault, BKF = Biabanak Fault, CHF = Chapedony Fault, DRF = Doruneh Fault, KBF = Kuhbanan Fault, KMF = Kalmard Fault, MAF = Mehdiabad Fault, MBF = Minab Fault, NAF = Nostratabad Fault, NHF = Nehbandan Fault, NNF = Nain Fault, RJF = Rafsanjan Fault, SBF = Shahre-Babak Fault, TKF = Taknar Fault, UZF = Uzbak-Kuh Fault, ZRF = Zarand Fault, ZTZ = Zagros Thrust Zone.

Please cite this article as: Malekzadeh Shafaroudi, A., et al., The Khopik porphyry copper prospect, Lut Block, Eastern Iran: Geology, alteration and mineralization, fluid inclusion, and oxygen isotope studies, Ore Geol. Rev. (2014), http://dx.doi.org/10.1016/j.oregeorev.2014.04.015

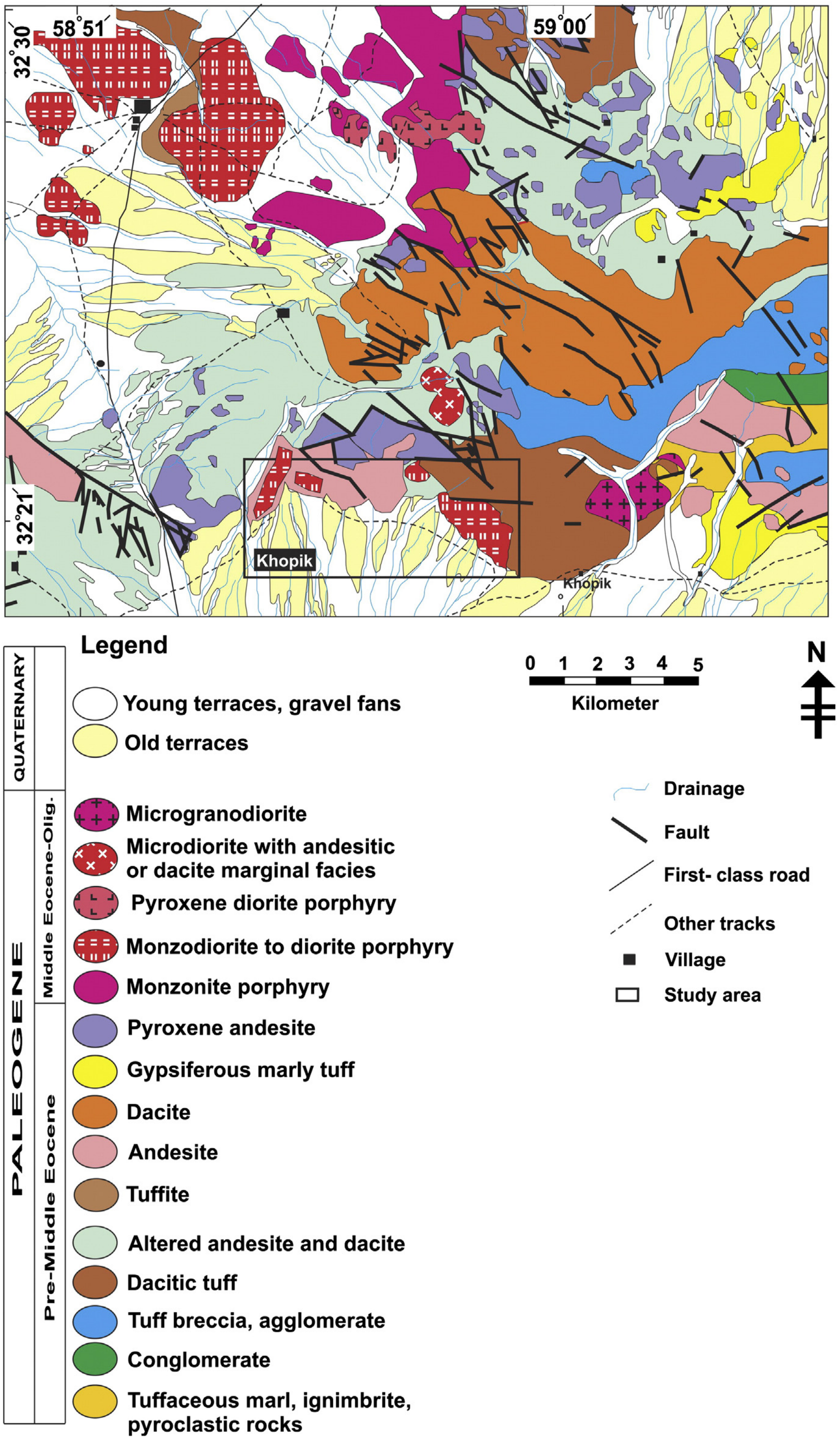

Fig. 2. Simplified regional geological map of study area modified after the Sar-e-Chah-e-Shur map (Geological Survey of Iran, 1975) and Mokhtaran map (Geological Survey of Iran, 1978). The location of prospect areas is shown in the inset.

Sheikhabad high-sulfidation and Hanich low-sulfidation gold deposits Karimpour, 2007; Fig. 2). In the study area, post-accretion magmatism commenced with the eruption of Eocene calc-alkaline volcanic rocks, closely followed by the emplacement of intermediate-acidic porphyritic intrusive rocks. The volcanic rocks predominantly consist of andesite and dacite lavas and tuffs, and the intrusive rocks vary from diorite to monzonite. Most of the volcanic and plutonic rocks are extensively altered and mineralized. The mineralization is closely associated with porphyritic subvolcanic intrusions. Phyllic, argillic, and propylitic alterations are the most common alteration types in the study area, and are associated with stockwork, disseminated, hydrothermal breccias, and vein-style mineralization.

Please cite this article as: Malekzadeh Shafaroudi, A., et al., The Khopik porphyry copper prospect, Lut Block, Eastern Iran: Geology, alteration and mineralization, fluid inclusion, and oxygen isotope studies, Ore Geol. Rev. (2014), http://dx.doi.org/10.1016/j.oregeorev.2014.04.015

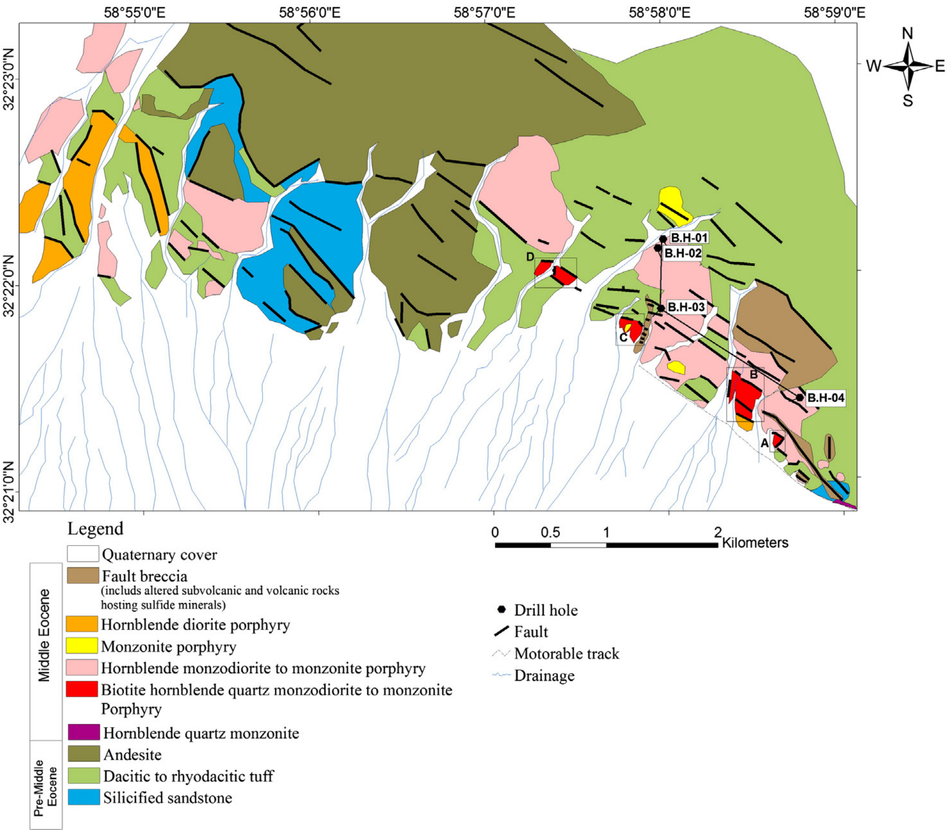

Fig. 3. Geologic map of the Khopik prospect area.

3. Geological setting of the Khopik prospect

3.1. Local geology

The major rock types in the Khopik area are Cenozoic calc-alkaline volcanic rocks and the spatially and temporally related subvolcanic intrusive stocks that are exposed along northwest-southeast oriented reverse faults (Figs. 3 and 4). The comagmatic volcanic rocks consist of dacitic to rhyodacitic and andesitic lavas (Fig. 3) that are extensively altered in the vicinity of the younger intrusive rock.

The subvolcanic intrusive rocks, the most dominant in the region, consist of five compositional groups, the relative ages of which can be established based on crosscutting relationships and alteration type as follows: 1) hornblende quartz monzonite; 2) biotite-hornblende quartz monzodiorite to monzonite porphyry; 3) hornblende monzonite to monzodiorite porphyry; 4) monzonite porphyry; and 5) hornblende diorite porphyry (Fig. 3). The ~ 39 Ma U-Pb radiometric ages obtained for the zircon from the host monzonite-diorite porphyries indicate a Middle Eocene age (Malekzadeh Shafaroudi, 2009).

3.2. The host subvolcanic monzonite-diorite porphyries

Hornblende quartz monzonite is the oldest intrusive rock and occurs in sparse, small outcrop in the eastern part of Khopik prospect (Fig. 3), and in drill hole BH–03 (Fig. 4A and B). Hornblende quartz monzonite consists of a medium-grained hypidiomorphic granular (Fig. 5A) groundmass consisting of andesine, K-feldspar, quartz, and hornblende. Phenocrysts ($\leq$70%) include andesine to andesine-oligoclase, K-feldspar, quartz, hornblende, and biotite (Fig. 5B). Magnetite and apatite are common accessory minerals. The monzonite is weakly to moderately altered, but is more strongly affected by potassic alteration with secondary biotite being a common mineral. The hornblende is replaced by the hydrothermal biotite, magnetite, calcite, and minor chlorite, with the hydrothermal orthoclase typically occurring in veinlet haloes. Potassic alteration contains both disseminated and stockwork sulfide ore.

Hornblende monzodiorite to monzonite porphyry is the most widely exposed intrusive rock in the study area (Figs. 3 and 4). It consists of ~ 35% phenocrysts, including 10–15% plagioclase, 8–10% K-feldspar, and 10–12% hornblende in a fine-grained groundmass (Fig. 5C). Accessory minerals are magnetite and apatite. This porphyry rock is extensively altered to chlorite, magnetite, epidote, calcite, quartz, minor sericite, and secondary biotite, and the alteration assemblage varies throughout the study area. Stockwork and disseminated sulfide mineralization is associated with magnetite. The Monzonite porphyry contains a phenocryst assemblage of 20–25% andesine and 15–20% K-feldspar (Fig. 5D). Sericite, quartz, and calcite are the main alteration minerals.

Hornblende diorite porphyry is the youngest intrusive rock and crops out mainly in the western part of the prospect (Fig. 3). The phenocrysts consist of 10–18% plagioclase, 1–2% K-feldspar, and 10–15% hornblende (Fig. 5E). Magnetite is an accessory mineral (3–4%). The hornblende diorite porphyry is unmineralized, but has undergone pervasive propylitic alteration, where hornblende phenocrysts are altered to chlorite, calcite, magnetite, and minor epidote.

4. Methods

More than 300 polished slabs and thin sections were prepared from the intrusive rock samples collected from surface and bore holes at the Khopik prospect for microscopic study. From these, thirteen least altered samples were selected for bulk rock analysis. Major elements were analyzed at the Ferdowsi University of Mashhad, using a Philips PW1480 X-ray spectrometer. Trace elements and REE analysis was carried out at ACME Laboratories of Canada using ICP-MS techniques following lithium metaborate/tetraborate fusion after nitric acid digestion. Metal concentrations were analyzed at ACME Laboratories of Canada and at AMDEL laboratory of Australia using ICP-MS techniques following hot Aqua

Please cite this article as: Malekzadeh Shafaroudi, A., et al., The Khopik porphyry copper prospect, Lut Block, Eastern Iran: Geology, alteration and mineralization, fluid inclusion, and oxygen isotope studies, Ore Geol. Rev. (2014), http://dx.doi.org/10.1016/j.oregeorev.2014.04.015

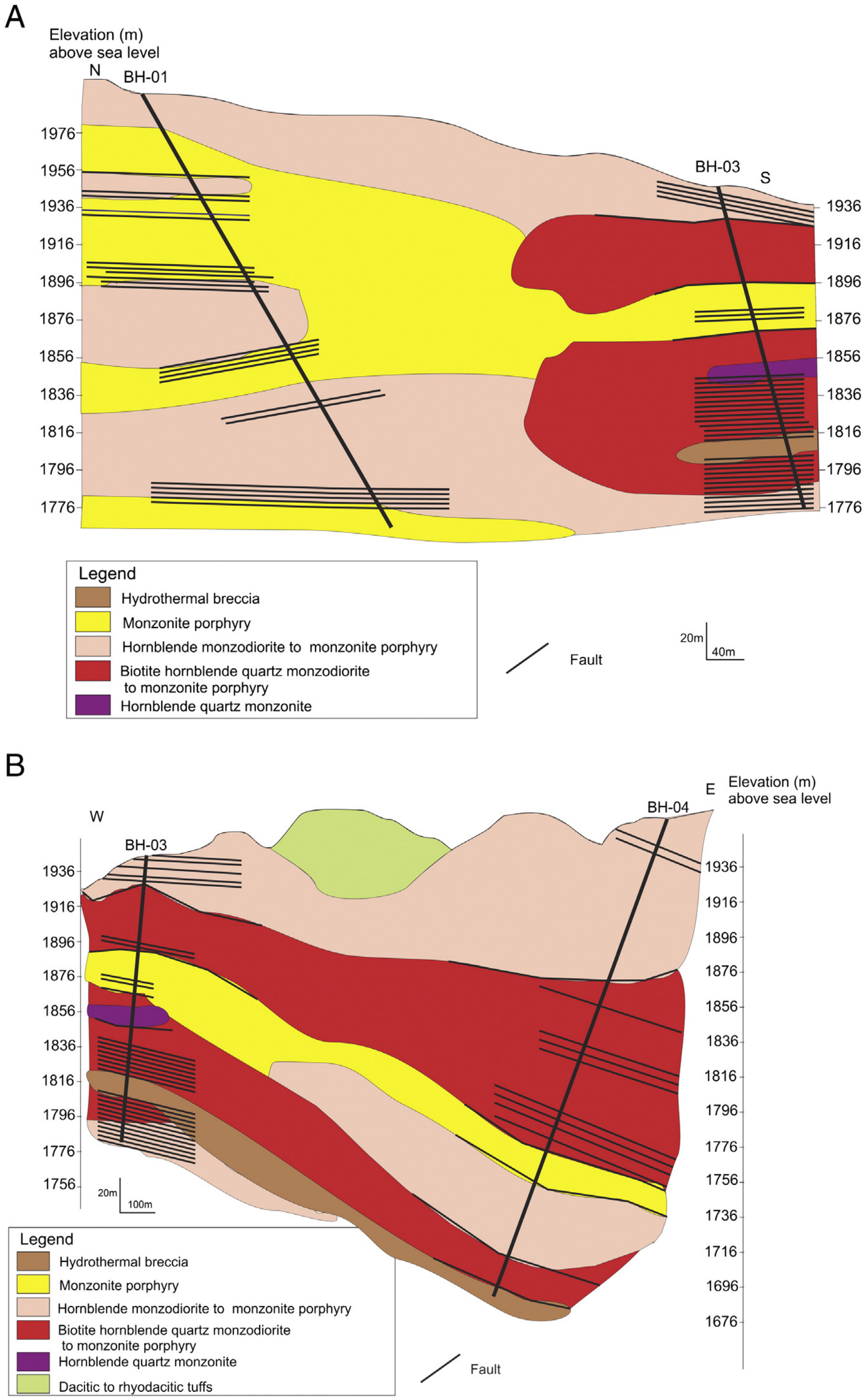

Fig. 4. A. Simplified geologic section between bore holes BH-01 and BH-03. B. Simplified geologic section between bore holes BH-03 and BH-04.

Regia digestion on 324 samples selected from surface and bore holes by the first author and by Pars Kani Company.

Nineteen doubly polished wafers (150 μm thick) prepared for fluid inclusion studies were examined petrographically. Eight wafers containing suitable fluid inclusions (>5 μm in size) from quartz in UST layers and in quartz-sulfide veinlets from potassic and QSCP alteration zones were selected for microthermometric measurements. The measurements were conducted on a Linkam THMSG 600 heating-freezing stage with temperature limits of 600 °C and −190 °C, and a precision of ±1.0 °C. The stage was calibrated at low temperatures with heptane (−90.6 ºC), chloroform (−63.0 ºC), chlorobenzene (−45.6 ºC), n-dodecane (−9.6 ºC) and distilled water (0.0 ºC). Calibration at 45 ºC was made with Merck melting point standard 9645, and at 306 ºC with sodium nitrate. Salinities and trapping pressure of fluid inclusions were calculated using the Microsoft Excel spreadsheet HOKIEFLINCS-H2O-NACL (Lecumberri-Sanchez et al., 2012; Steele-MacInnis et al., 2012) and the algorithm of Brown and Lamb FLINCOR program (1989).

Six quartz samples from UST and quartz-sulfide veinlets were analyzed for stable oxygen isotope compositions after careful hand picking and purification at the Institute of Mineralogy and Geochemistry, University of Lausanne, Switzerland. Oxygen isotopic measurements were obtained using protocols from Sharp (1990), Rumble and Hoering

Please cite this article as: Malekzadeh Shafaroudi, A., et al., The Khopik porphyry copper prospect, Lut Block, Eastern Iran: Geology, alteration and mineralization, fluid inclusion, and oxygen isotope studies, Ore Geol. Rev. (2014), http://dx.doi.org/10.1016/j.oregeorev.2014.04.015

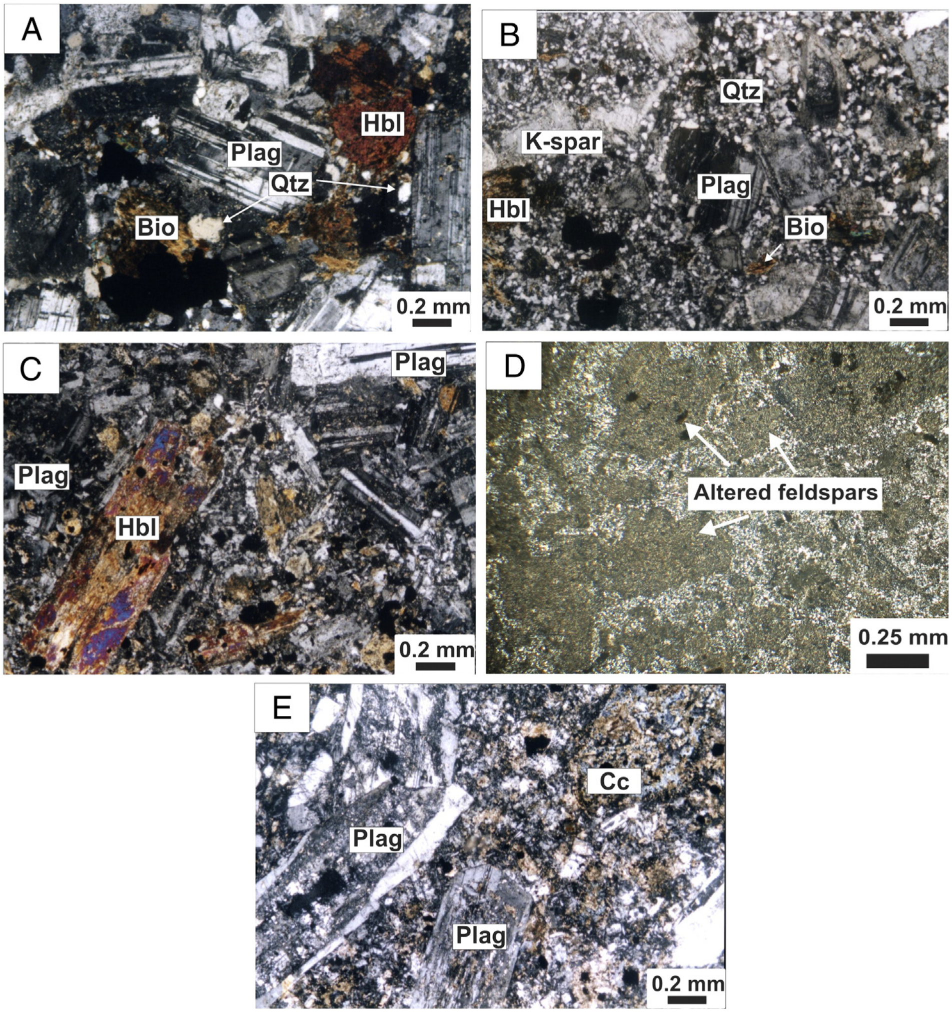

Fig. 5. Photomicrograph of A. Hornblende quartz monzonite with coarse-grained hypidiomorphic granular texture showing plagioclase, hornblende, quartz, opaque minerals, and minor secondary biotite (KH–1 sample). B. Biotite-hornblende quartz monzodiorite to monzonite porphyry (KH–84 sample). C. Hornblende monzodiorite to monzonite porphyry showing plagioclase, hornblende, and opaque minerals (KH–13 sample). D. Hornblende monzonite porphyry affected by QSCP alteration overprinted by supergene argillic zone (KH–5–B1 sample). E. Hornblende diorite porphyry with carbonate- chlorite alteration (KH–110 sample). Qtz = quartz, Hbl = hornblende, Bio = biotite, Cc = calcite, K-spar = K-feldspar, and Plag = plagioclase.

(1994), and Kasemann et al. (2001). The V-SMOW ($\delta^{18}O$ SMOW) values were established relative to an internal standard NBS–28 quartz ($\delta^{18}O = 9.64 \pm 0.06$ ‰).

5. Geochemistry of the host intrusive rocks

The major, trace and REE contents of the host porphyries are shown in Table 1. On the $K_2O + Na_2O$ versus SiO_2 diagram, the samples plot in the field of gabbro diorite, diorite, monzonite, quartz monzonite, and granodiorite (Fig. 6A). Magnetic susceptibility of these intrusions being between 1500×10^{-5}–6000×10^{-5} SI confirms their provenance from magnetite-series granitic rocks (Fig. 6B). The Nb, Yb, Rb, Ta, and Y values and low ratio of Nb/Y (0.16–0.46) and Ta/Yb (0.12–1.9) fall within the volcanic arc granite (VRG) field of Pearce et al. (1984) and Forster et al. (1997) and indicate that the intrusions were formed in a volcanic arc system. This is confirmed by enrichment in LILE, such as Rb, Ba, K, and Cs, and depletion in HFSE, such as Nb, Ti, Ta, Zr, and Y. However, high Sr concentrations ($\leq$500 ppm) indicate geochemical characteristics different from a typical volcanic arc granite. In the Sr/Y versus Y diagram, most samples plot in the adakite field and only two samples plot within the classic island arc andesites (Fig. 7). Despite some chemical affinities with adakites, the intrusive rocks have chemical signatures distinct from normal adakites, including their higher K_2O and K_2O/Na_2O ratios, lower Mg#, $(La/Yb)_N$ and $(Ce/Yb)_N$, moderate LREE, and relatively moderate HREE contents (Table 1). Their initial $^{87}Sr/^{86}Sr$ and $^{143}Nd/^{144}Nd$ ratios (Malekzadeh Shafaroudi et al., 2010) are 0.7047–0.7048, and 0.512694–0.512713 (ε_{Ndi} of +1.45 to +1.81), respectively. These chemical characteristics suggest that the parental magma of the intrusive rocks at Khopik area was derived from continental mantle lithosphere (Malekzadeh Shafaroudi et al., 2010).

We conclude that the host intrusive rocks are metaluminous I-type, magnetite-series, with high-K calc-alkaline to shoshonitic composition that likely formed in a continental arc setting at a convergent plate boundary. Partial melting of the mantle modified by hydrous, silica-rich slab-derived melts, and/or input of enriched mantle-derived ultra-potassic magmas during or prior to the formation and migration of melts could explain the high initial K_2O contents and high K_2O/Na_2O ratios of the host rocks, similar to scenarios presented by Esperanca et al. (1992), Müller and Groves (1993), and Zhang et al. (2001).

6. Alteration and mineralization

Based on field and laboratory results, the alteration intensity of the host rocks is represented by three groups of strongly (□ 50%), moderately (30–50%), and weakly altered rocks (□ 30%) altered rocks. Hydrothermal alteration has affected all exposed volcanic and subvolcanic

Please cite this article as: Malekzadeh Shafaroudi, A., et al., The Khopik porphyry copper prospect, Lut Block, Eastern Iran: Geology, alteration and mineralization, fluid inclusion, and oxygen isotope studies, Ore Geol. Rev. (2014), http://dx.doi.org/10.1016/j.oregeorev.2014.04.015

Table 1
Major, trace, and REE elements analysis of least–altered monzonitic syn-mineralization intrusive rocks from the Khopik prospect area.

Wt%	MA-52	MA-67	MA-130	MA-178	MA-87	MA-95	MA-93	MA-126	MA-163	KH-1	KH-88	KH-89	KH-108
SiO_2	62.41	62.25	58.76	54.90	62.42	57.77	62.25	57.89	55.87	58.75	64.76	58.19	55.93
TiO_2	0.47	0.52	0.53	0.75	0.44	0.58	0.51	0.58	0.61	0.41	0.39	0.44	0.53
Al_2O_3	14.61	14.70	15.15	16.15	14.12	14.49	15.39	15.11	15.84	14.91	14.65	15.73	15.33
FeOT	5.76	6.98	7.13	9.13	5.65	6.52	4.90	7.11	7.45	6.85	5.84	6.11	7.70
MnO	0.17	0.22	0.24	0.26	0.17	0.27	0.09	0.18	0.19	0.12	0.08	0.13	0.21
MgO	1.87	1.87	2.17	3.59	1.52	2.81	1.46	1.93	2.79	2.02	1.54	2.11	3.08
CaO	5.36	5.55	7.31	8.90	4.50	7.65	4.35	7.32	7.30	6.64	4.30	6.49	7.81
Na_2O	3.31	3.62	3.52	3.33	3.70	3.04	3.17	3.30	3.85	3.29	3.20	4.65	3.22
K_2O	4.38	4.03	2.40	2.00	4.43	3.46	4.31	2.59	3.05	3.48	3.03	3.03	2.50
P_2O_5	0.27	0.27	0.36	0.37	0.29	0.44	0.29	0.38	0.48	0.20	0.18	0.24	0.37
L.O.I	1.41	1.51	2.59	0.85	0.81	3.53	2.12	2.35	1.86	1.56	1.48	1.08	3.18
Total	100.02	101.52	100.16	100.23	98.05	100.56	98.84	98.74	99.29	98.23	99.45	98.20	99.86
K_2O/Na_2O	1.32	1.11	0.68	0.60	1.20	1.14	1.36	0.78	0.79	1.06	0.95	0.65	0.77
Mg#	0.37	0.32	0.36	0.42	0.32	0.44	0.35	0.33	0.41	0.35	0.32	0.39	0.42
ppm													
V	168	190	174	274	157	219	174	176	205	146	135	148	204
Cr	83	54	24	22	44	29	114	25	15	43	28	36	24
Mn	1087	1271	1560	1781	976	1603	536	1033	1273	744	502	770	1288
Co	17	20	14	28	16	18	13	17	20	16	11	15	22
Ni	33	31	30	29	30	32	29	30	27	27	26	24	31
Cu	100	98	11	47	281	26	64	16	43	25	1979	54	63
Zn	205	223	82	111	276	252	227	26	59	n.d	21	17	40
Cs	3.2	5.6	2.7	3.1	3.6	2.6	4.8	3.0	1.2	3.9	6.4	3.7	6.4
Ba	1068	1040	974	892	1074	1104	1133	1109	1041	1220	1153	1232	1121
Rb	121	109	38	29	145	56	130	57	57	79	84	85	56
Sr	720	630	1018	550	660	875	1730	905	802	718	541	675	760
Y	14	14	17	19	13	17	15	16	20	13	10	11	16
Zr	93	90	92	44	85	95	170	98	91	83	84	97	75
Nb	4	4	4	3	4	4	4	4	4	5	4	5	3
Hf	1.5	1.7	0.9	1.9	0.9	0.8	2.1	1.5	2.4	1.0	0.7	2.0	1.5
Ta	0.4	0.4	0.3	0.5	0.3	0.3	0.8	0.4	0.4	2.0	1.3	2.8	0.3
Pb	69.9	46.2	12	8.3	36.7	76.3	61.9	7.5	13.6	10.4	10.1	9.4	9.6
Th	10.1	9.8	4.3	3.3	10.6	8.2	10.7	3.9	5.5	6.1	4.8	5.8	4.1
U	2.7	2.7	1.1	0.7	2.3	1.8	3.0	1.1	1.6	1.1	1.0	0.8	1.1
La	23.2	23.8	19.9	16.5	23.0	26.1	26.8	20.2	25.3	17.7	13.6	17.1	20.8
Ce	45.0	45.0	41.3	37.2	43.4	56.6	50.1	42.7	53.6	32.4	26.0	34.6	42.9
Pr	5.31	5.30	5.27	5.04	5.03	6.35	5.71	5.26	6.56	3.79	3.02	3.98	5.38
Nd	20.3	21.7	20.6	21.5	19.3	27.1	23.7	22.6	27.3	14.2	12.2	15.4	19.8
Sm	4.07	4.17	4.11	4.69	3.66	5.57	4.59	4.52	5.75	2.88	2.54	3.35	4.50
Eu	1.08	1.07	1.19	1.28	0.93	1.31	1.16	1.28	1.43	0.77	0.69	0.95	1.19
Gd	3.51	3.64	3.71	4.45	3.37	4.59	3.92	3.88	4.95	2.59	2.11	3.09	3.67
Tb	0.58	0.60	0.62	0.81	0.57	0.72	0.58	0.60	0.81	0.41	0.34	0.46	0.69
Dy	2.56	2.87	3.11	3.73	2.48	3.37	2.86	3.09	4.08	2.35	1.89	2.36	3.08
Ho	0.56	0.55	0.70	0.95	0.55	0.70	0.62	0.64	0.96	0.51	0.38	0.48	0.67
Er	1.66	1.68	1.75	2.15	1.32	1.85	1.70	1.96	2.26	1.37	1.14	1.40	1.83
Tm	0.23	0.25	0.30	0.38	0.25	0.29	0.28	0.29	0.35	0.19	0.18	0.25	0.29
Yb	1.71	1.69	2.03	2.23	1.60	1.88	1.82	1.91	2.44	1.49	1.18	1.48	2.01
Lu	0.29	0.29	0.28	0.39	0.26	0.27	0.29	0.30	0.41	0.23	0.18	0.25	0.31
Sr/Y	51.4	45.0	59.9	29.0	50.8	51.5	115.3	56.6	40.1	55.2	54.1	61.4	47.5
Eu/Eu*	0.87	0.84	0.93	0.85	0.81	0.79	0.83	0.93	0.82	0.86	0.91	0.90	0.89
$(La/Yb)_N$	9.14	9.49	6.60	4.98	9.69	9.36	9.92	7.13	6.99	8	7.77	7.79	6.97
$(Ce/Yb)_N$	6.80	6.88	5.26	4.31	7.01	7.78	7.12	5.78	5.68	5.62	5.69	6.04	5.52

Mg# = Mg/Mg + Fe^{2+}.
$(La/Yb)_N$ = La normalized by chondrite/Yb normalized by chondrite.
$(Ce/Yb)_N$ = Ce normalized by chondrite/Yb normalized by chondrite.
[*] X-ray fluorescence analysis of major elements was performed at the Ferdowsi University of Mashhad, using a Philips PW1480 X-ray spectrometer. Trace elements and REE analyses were carried out at the ACME laboratory of Canada using ICP-MS and the following lithium metaborates/tetraborates fusion and nitric acid digestion of a 0.2 g sample.

rocks at Khopik prospect in an area of 14 km^2. Hypogene alteration includes potassic, sericitic-potassic, quartz-sericite-carbonate-pyrite (QSCP), quartz-carbonate-pyrite (QCP), and propylitic zones (Fig. 8). Styles of mineralization include disseminated, stockwork, minor hydrothermal breccia, and veins. Stockwork ore is the most relevant type and is mainly found in a ~ 7 km^2 area in the eastern part of the prospect. The distribution and density of veins in relation to alteration zones is shown in Fig. 9. Vein and veinlet density at Khopik (Fig. 10A and B) are based on drill holes BH–01, BH–03, and BH–04 and subsurface alteration zones. They were mapped using an Anaconda-style system where linear mapping records the average width and spacing of veinlets, which allows direct calculation of the volume % of veinlets in a rock (Redmond and Einaudi, 2010). Veinlet density is displayed in two ranges from 15–30 and 5–15 veins per m^2, and the alteration intensity is shown using three different patterns.

Chalcopyrite, minor bornite, sphalerite, and galena are the main hypogene sulfide minerals. Modal abundances of sulfide minerals, mostly pyrite and chalcopyrite, are presented in five ranges from < 1% to 30–35%. Sulfides are largely oxidized to malachite, hematite, goethite, and limonite near the surface.

Unidirectional solidification texture zones (UST). Layered comb-quartz textures, referred to as UST (Kirkham and Sinclair, 1988; Zaraisky et al.,

Please cite this article as: Malekzadeh Shafaroudi, A., et al., The Khopik porphyry copper prospect, Lut Block, Eastern Iran: Geology, alteration and mineralization, fluid inclusion, and oxygen isotope studies, Ore Geol. Rev. (2014), http://dx.doi.org/10.1016/j.oregeorev.2014.04.015

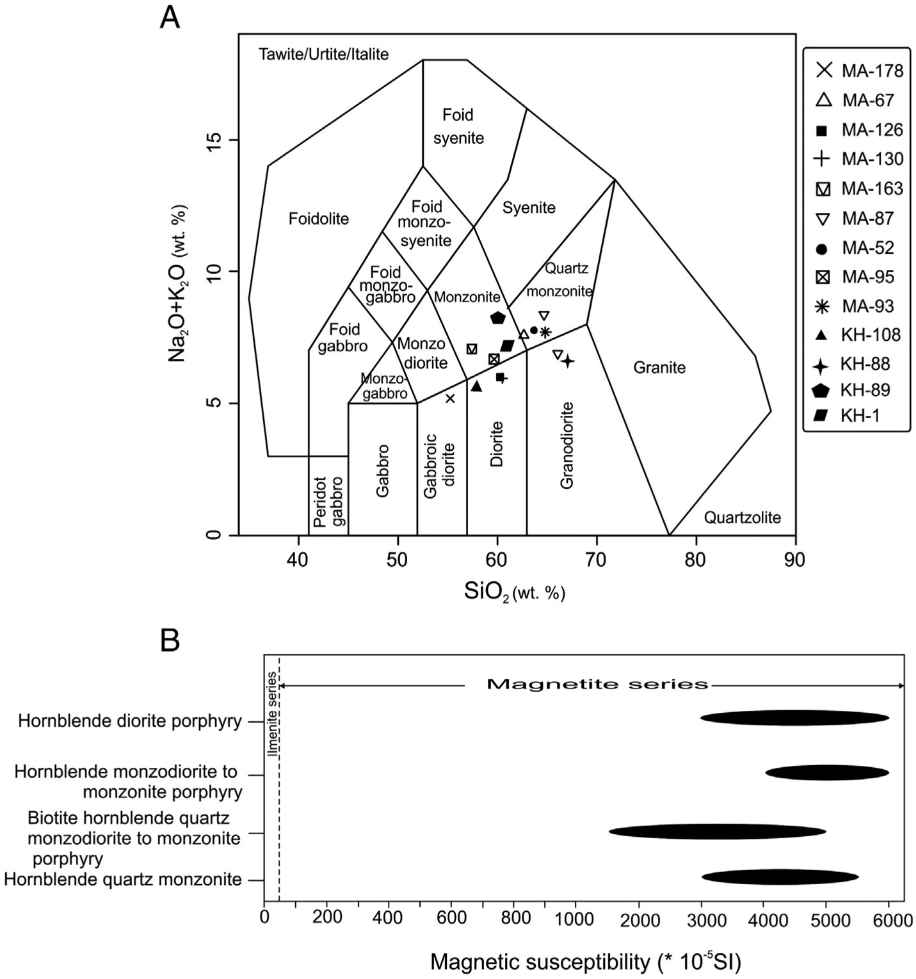

Fig. 6. A. Classification of syn-mineralization intrusions of the Khopik area in $Na_2O + K_2O$ versus SiO_2 diagram of Middlemost (1985). Khopik samples plot in the field of monzonite, quartz monzonite, granodiorite, diorite and gabbroic diorite. B. Rock magnetic susceptibility of the Khopik area (from Malekzadeh Shafaroudi, 2009).

1997) can be observed on the surface in area "D" (Fig. 8) within the biotite-hornblende quartz monzodiorite to monzonite porphyry. The UST zones are composed of irregular sub-parallel layers of quartz crystals with orientated C-axis terminations. Prismatic quartz crystals are oriented roughly perpendicular to the planes of layering and appear to have grown on a crystallized igneous substrate with an aplitic texture, inward toward the center of the intrusion (Harris et al., 2004). The layers generally range from □1 mm to several centimeters, or more, in thickness and are separated by an interlayer of fine-grained, aplitic monzonite. They are significant because individual layers likely crystallized from boundary layers of exsolved magmatic fluid evidencing volatile separation (Harris et al., 2004). The development of multiple layers reflects a continuous supply of magmatic fluid from subjacent magma (Lowenstern and Sinclair, 1996). Seedorff and Einaudi (2004) and Seedorff et al. (2005) suggested that there is a close relationship between UST layers and "A" veins (earliest formed veinlets in porphyry copper deposit; see Gustafson and Hunt, 1975) in some porphyry copper and molybdenum deposits, in that both textures can locally be seen to coalesce.

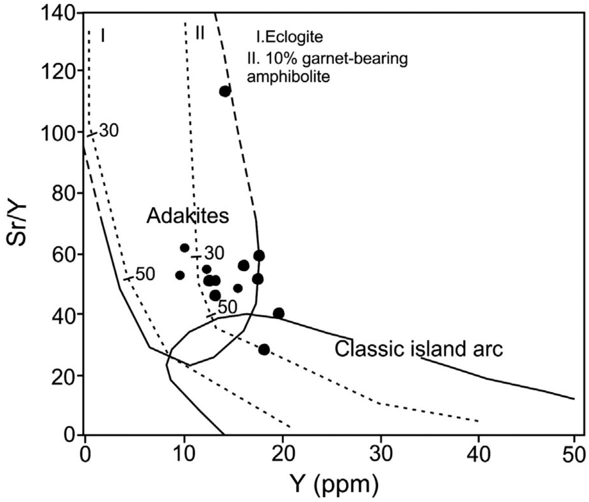

Fig. 7. Syn-mineralization intrusions of the Khopik area mostly plot in the field of adakites, with higher Sr/Y than classic island arc in Sr/Y versus Y diagram of Defant and Drummond (1990).

At Khopik prospect, these textures define alternating bands (<1 cm thick) of coarse-grained prismatic quartz, and intergrowths of biotite, pyrite, chalcopyrite, and sugary quartz-feldspar (aplitic porphyry) rimming the triangular quartz crystals (Figs. 11 and 12). Intergrowths of pyrite and chalcopyrite associated with UST may reflect the earliest stage of sulfide mineralization. On the other hand, there are obvious textural differences between the different layers of the UST. This is expressed in a clear progression of the degree of crystallization of the magma with time, in which both the percentage of phenocrysts and the average grain size of the groundmass increased with time (Fig. 12). The upper early layer contains about 30% phenocrysts (plagioclase, K-feldspar, biotite, and hornblende), a fine-grained groundmass with an average grain size of 0.02 mm. In the later middle layer, the grain size of the groundmass

Please cite this article as: Malekzadeh Shafaroudi, A., et al., The Khopik porphyry copper prospect, Lut Block, Eastern Iran: Geology, alteration and mineralization, fluid inclusion, and oxygen isotope studies, Ore Geol. Rev. (2014), http://dx.doi.org/10.1016/j.oregeorev.2014.04.015

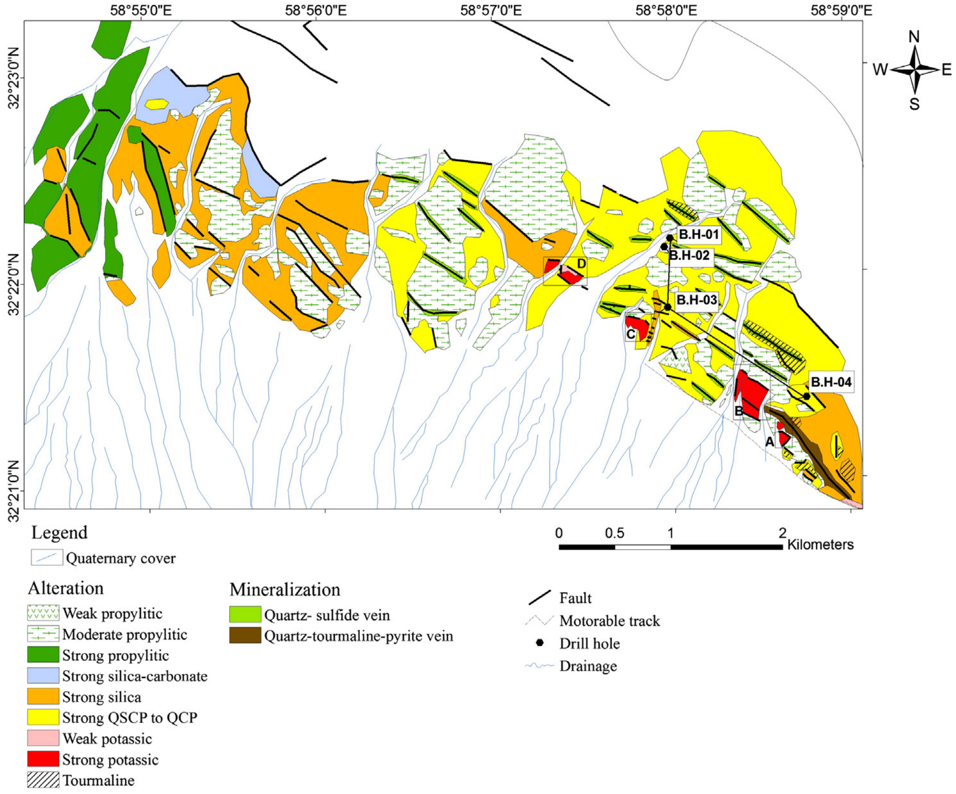

Fig. 8. Alteration map of the Khopik prospect area.

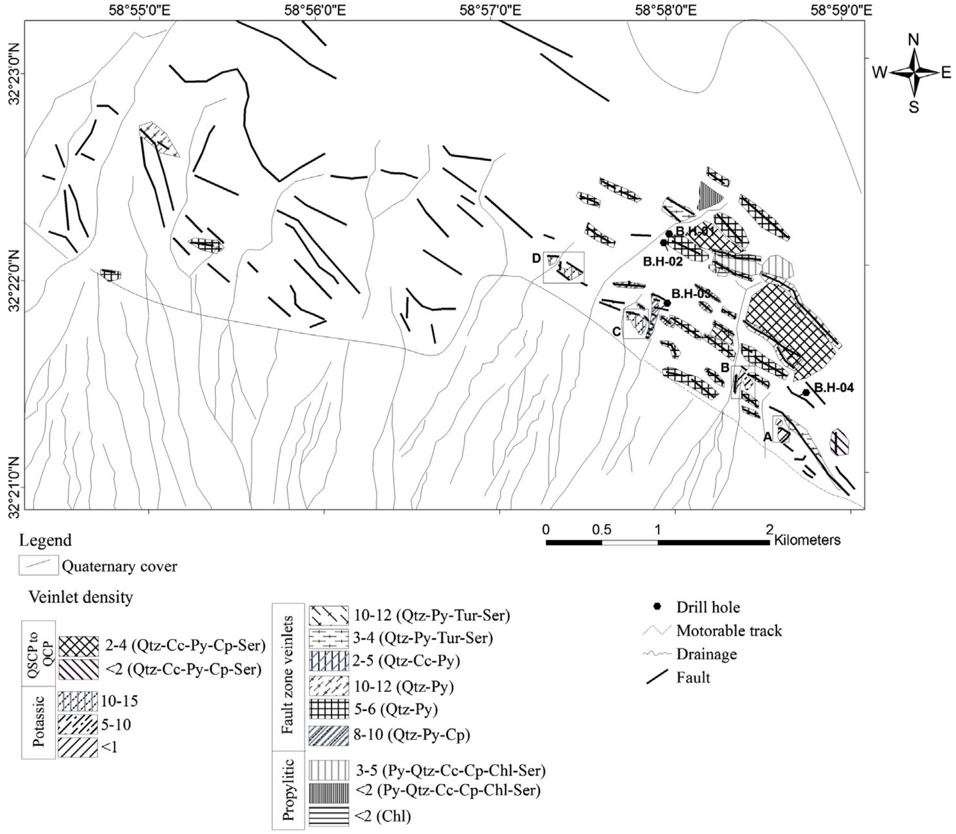

Fig. 9. Veinlet density map of the Khopik prospect area. Py = pyrite, Qtz = quartz, Tur = tourmaline, Ser = sericite, Cc = calcite, Cp = chalcopyrite, and Chl = chlorite.

Please cite this article as: Malekzadeh Shafaroudi, A., et al., The Khopik porphyry copper prospect, Lut Block, Eastern Iran: Geology, alteration and mineralization, fluid inclusion, and oxygen isotope studies, Ore Geol. Rev. (2014), http://dx.doi.org/10.1016/j.oregeorev.2014.04.015

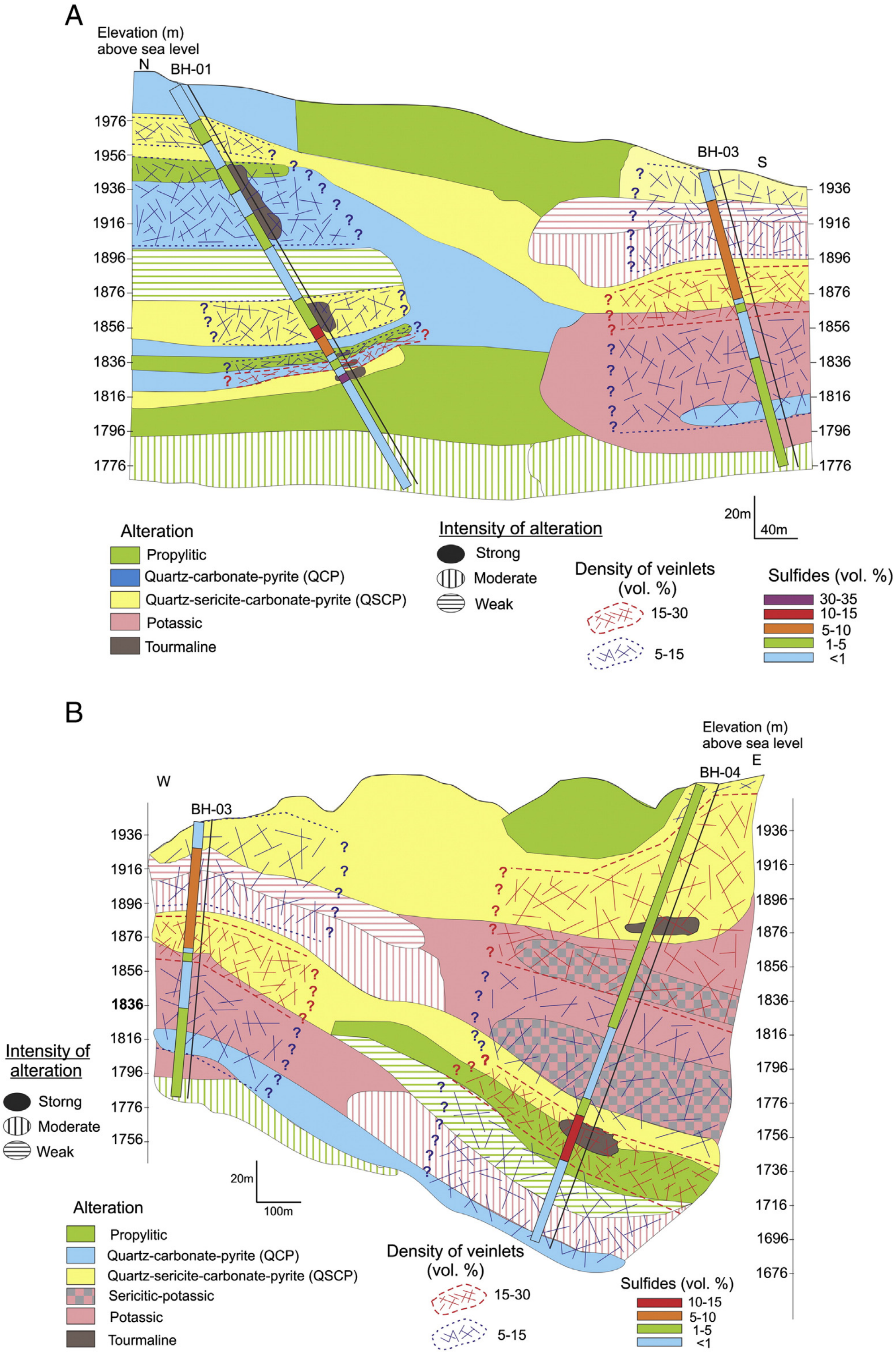

Fig. 10. A. Alteration, veinlet density, and sulfides percent section between bore holes BH–01 and BH–03. Alteration intensity is shown using three different patterns. Veinlet density is displayed in two ranges from 15–30 and 5–15 veins per m^2. B. Alteration, veinlet density, and sulfides percent section between bore holes BH–03 and BH–04. Alteration intensity is shown using three different patterns. Veinlet density is displayed in two ranges from 15–30 and 5–15 veins per m^2.

is about 0.04 mm. Here, many small phenocrysts, about 40%, grew from groundmass. The youngest lower layer displays the coarsest groundmass with about 0.1 mm grain size and 50% phenocrysts.

Potassic alteration associated with the formation of abundant sulfide veinlets and Cu-Au mineralization is the oldest alteration events and occurs only in the hornblende quartz monzonite, and biotite-hornblende quartz monzodiorite to monzonite porphyry. The potassic alteration zone was identified in only four places (shown as A to D in Fig. 8) on the surface, and in the bore holes (BH–03 and BH–04; Fig. 10A and B). Typical whole rock Cu contents were 0.02–2 wt. %, Au < 0.1– 0.9 ppm, Mo < 70 ppm, Zn < 50–244 ppm, and Pb < 20–97 ppm in forty two d samples.

The dominant mineral assemblage in the potassic zone is biotite (2–50%, and <30–50% in intensely altered rocks), K-feldspar (5–6%),

Please cite this article as: Malekzadeh Shafaroudi, A., et al., The Khopik porphyry copper prospect, Lut Block, Eastern Iran: Geology, alteration and mineralization, fluid inclusion, and oxygen isotope studies, Ore Geol. Rev. (2014), http://dx.doi.org/10.1016/j.oregeorev.2014.04.015

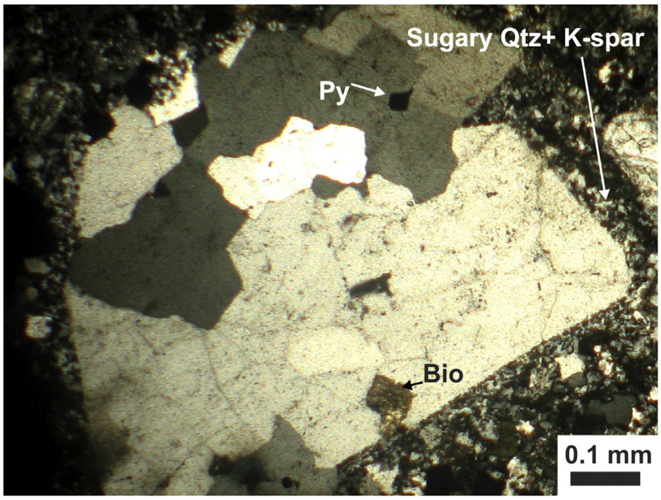

Fig. 11. Photograph showing Coarse-grained prismatic UST quartz and biotite and sugary quartz-feldspar of aplitic textured porphyry rimming the triangular quartz crystals.

quartz (5–50%), magnetite (<3%), calcite (10–15%), minor sericite with subordinate anhydrite, chlorite, hematite, and clay minerals. At this stage, plagioclase phenocrysts were replaced by K-feldspar, and amphibole phenocrysts by an aggregate of biotite and magnetite. Biotite occurs as euhedral grains (□ 1 mm), as patchy replacements of the primary hornblende, or as subhedral to anhedral grains (0.1–0.8 mm) within veinlets and pseudomorphic aggregates (0.1–0.5 mm). Under plane polarized light the euhedral biotite is greenish brown to brown, brown to pale brown in veinlets, and light brown with greenish shades in pseudomorphic aggregates after hornblende phenocrysts. K-feldspar occurs as partially to completely replacing the phenocrysts within veinlets, and as pervasive alteration in the groundmass. K-feldspar is euhedral to anhedral (≥1 cm long) with a pale brown-pink hue under the microscope. Also, it occurs as fine-grained granular crystals in the groundmass extending into the plagioclase phenocrysts via microfractures and cleavage planes. Quartz and calcite are common, either as veinlets, or as replacement of mafic minerals and plagioclase. The density of veinlets is high and reaches ≥ 15 veinlets/m^2 on the surface exposures and 30 veinlets/m^2 in bore holes (Figs. 9 and 10). Seven veinlet types (0.1–5 cm thick) are recognized based on their mineralogy, whereas biotite and quartz-carbonate-pyrite veinlets are most abundant (Table 2). Sulfides comprise □ 8% and rarely > 15% of the rock volume as in BH–04 at 253.8–275.3 m. Pyrite, the earliest-formed sulfide, and the later chalcopyrite intergrown with minor bornite, are the main ore minerals that occur with some magnetite in both pervasively altered porphyries, as well as in stockworks. The mineral paragenetic sequence in the potassic zone is shown in Figs. 13 and 14A to E.

Sericitic-potassic alteration locally occurs on surface exposures of dacite and rhyodacite, and in biotite-hornblende quartz monzodiorite to monzonite porphyry in the drill hole BH–04, where its intensity is weak to moderate (Figs. 8 and 10A).

The alteration assemblage consists of ~ 1% biotite and ~ 4% sericite. The secondary biotite and sericite are interpreted to have formed by two temporally distinct events in the transition zone between the potassic and the quartz-sericite-carbonate-pyrite alterations. The intrusive rocks affected by this alteration contain 5–7% biotite, 15–25% sericite, 10–12% calcite, 30% quartz, and minor magnetite. Biotite, calcite, and sericite mainly occur as veinlets and as replacements of mafic minerals and plagioclase.

Disseminated and stockwork pyrite, chalcopyrite, and minor magnetite are associated with sericitic-potassic alteration zone. The volcanic rocks contain only ~1% disseminated sulfides, pyrite and chalcopyrite, and the intrusive rocks 1–5%. The highest vein density, observed in

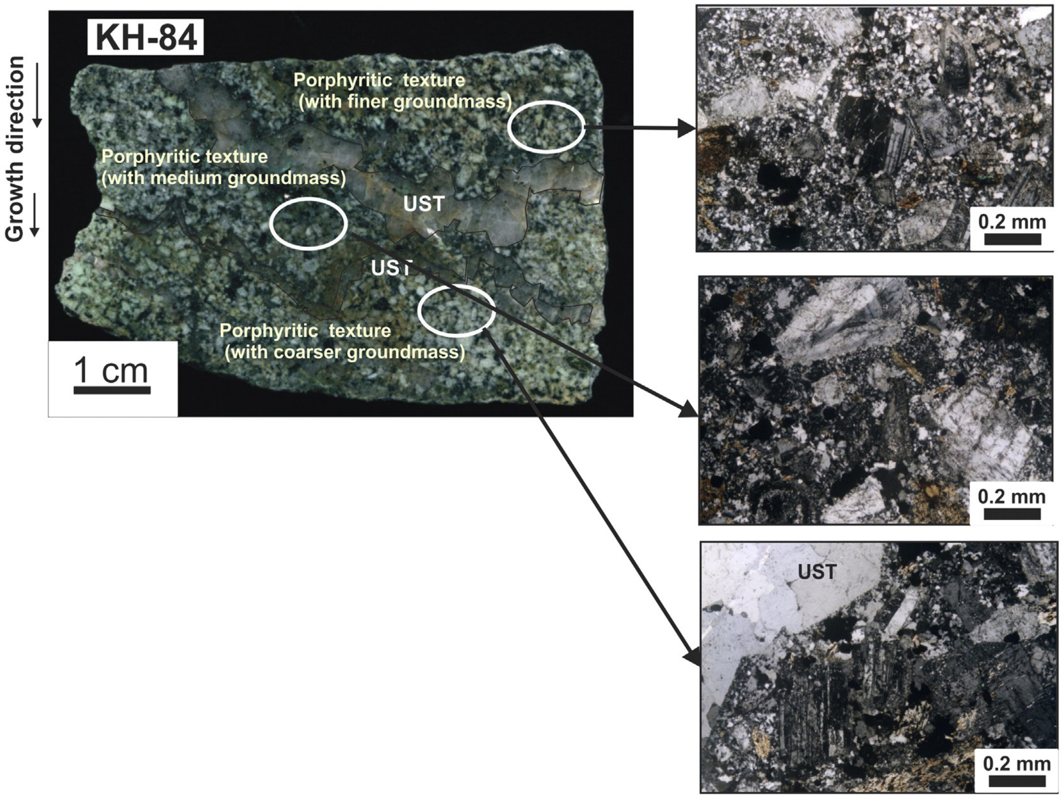

Fig. 12. Textural variations between different layers of the UST at the Khopik area.

Please cite this article as: Malekzadeh Shafaroudi, A., et al., The Khopik porphyry copper prospect, Lut Block, Eastern Iran: Geology, alteration and mineralization, fluid inclusion, and oxygen isotope studies, Ore Geol. Rev. (2014), http://dx.doi.org/10.1016/j.oregeorev.2014.04.015

Table 2
Summary of characteristics of hypogene alteration zones and types of veins and veinlets associated with them.

Alteration type	New (added) minerals	Relict minerals	Types of veinlets	Width (mm)	Abundance
Potassic	Bio + Kspar + Qtz + Mt + Cc	Qtz + Plag + Kspar + Bio + Hbl ± Mt ± Apa	-Bio	1	C
			-Qtz-Cc ± Py ± Cp ± Mt ± Bn ± Bio	0.5-40	C
			-Qtz-Cp-Bn	0.5-50	C
			-Qtz-Py-Cp ± Kspar ± Mt	1-30	R
			-Mt-Bio-Kspar-Qtz	2	R
			-Qtz-Py-Cp-Mt ± Bio	3-30	R
			-Qtz-Kspar-Bio	0.1-0.3	VR
Sericitic-potassic	Bio + Ser + Qtz + Cc ± Mt	Qtz + Plag + Kspar + Bio + Hbl ± Mt ± Apa	-Qtz-Cc-Py ± Ser	10-12	C
			-Qtz-Cp	1-5	C
			-Qtz-Py-Cp-Mt	2-7	VR
Quartz-sericite-carbonate-pyrite	Qtz + Ser + Cc + Py ± Tur	Qtz + Plag + Kspar ± Hbl ± Mt ± Apa	-Qtz-Cc-Py-Cp ± Ser	4-6	C
			-Tur-Py-Cp ± Bn ± Qtz ± Ser ± Cc	0.5-20	C-VR
			-Qtz-Cp-Py-Mt ± Cp	5-10	R
			-Qtz-Py-Cc-Ser-Cp-Mt-Bn	1-5	R
			-Ser	0.1-0.6	VR
			-Cp	1-4	VR
Quartz-carbonate-pyrite	Qtz + Cc + Py ± Tur	Qtz + Plag + Kspar ± Hbl ± Mt ± Apa	Mineralization associated with this zone is mainly hydrothermal breccia. Veinlets of Cc-Py crosscut fragments and cement of hydrothermal breccia and formed after brecciation. In subvolcanic intrusive rocks, mineralization is stockwork and 4 types of veinlets is recognized:		
			-Qtz-Cc-Py ± Cp ± Tur ± Sl	0.4-12	C-VR
			-Cc-Py	0.1-0.6	VR
			-Mt-Qtz-Tur-Cc ± Py ± Cp	10-15	VR
			-Qtz-Py-Cp-Bn-Mt ± Sl	0.1-0.5	VR
Propylitic	Qtz + Chl + Epi + Cc + Mt ± Ser ± Tur	Plag + Hbl ± ± Qtz ± Mt	-Py-Qtz-Cc ± Cp ± Chl ± Ser	0.2-3	C-VR
			-Chl	0.05	VR
			-Qtz-Chl-Cp	0.2	VR
			-Qtz-Tur-Py ± Cp ± Bn ± Chl	0.3-1	VR
			-Qtz-Py-Chl-Mt ± Cc	0.1-0.3	VR
			-Cc-Epi-Chl	0.1-0.4	VR
			-Act	0.2	VR

Abbreviations: Qtz = Quartz, Py = Pyrite, Cp = Chalcopyrite, Bio = Biotite, Cc = Calcite, Kspar = K-feldspar, Plag = Plagioclase, Hbl = Hornblende, Apa = Apatite, Mt = Magnetite, Bn = Bornite, Ser = Sericite, Tur = Tourmaline, Sl = Sphalerite, Chl = Chlorite, Epi = Epidote, and Act = Actinolite.
C = common, R = rare, and VR = very rare.

129–137 m interval in the drill hole BH–04 (Fig. 10B), is 15–30 veinlets/m^2. Copper and gold ore grades in twenty samples (Cu < 200 ppm, Au < 20 ppb, Mo < 9 ppm, Zn < 60 ppm, and Pb < 8 ppm) are lower than in the potassic alteration zone.

Three types of veinlets (1–12 mm thick) including quartz-calcite-pyrite ± sericite, quartz-chalcopyrite, and quartz-pyrite-chalcopyrite-magnetite are recognized in this alteration zone (Table 2) with the first type being most abundant. The mineral paragenesis in the sericitic-potassic zone is shown in Fig. 13.

Quartz-sericite-carbonate-pyrite (QSCP) alteration is exposed in the eastern part of the Khopik prospect (Fig. 8), where it is difficult to discriminate from the quartz-carbonate-pyrite zone (see below). The QSCP can

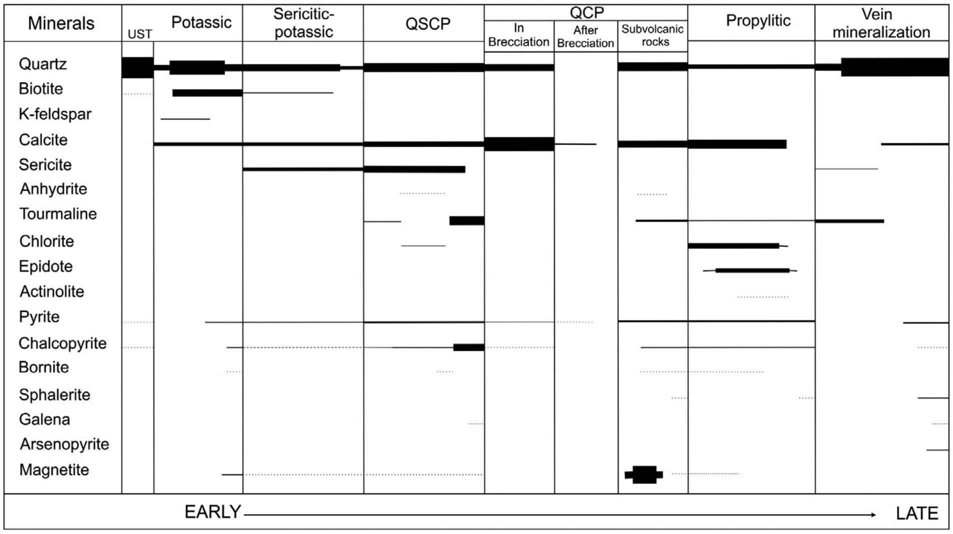

Fig. 13. Paragenetic mineral assemblages in the Khopik area.

Please cite this article as: Malekzadeh Shafaroudi, A., et al., The Khopik porphyry copper prospect, Lut Block, Eastern Iran: Geology, alteration and mineralization, fluid inclusion, and oxygen isotope studies, Ore Geol. Rev. (2014), http://dx.doi.org/10.1016/j.oregeorev.2014.04.015

be distinguished by its white to yellow color and its intensity in some drill holes completely obliterating the original igneous textures (Figs. 8, 10A and B). The QSCP alteration consists of veinlets and replacement zones of quartz (25–50%), sericite (30–35%), calcite (3–40%), and pyrite (4–5%), as well as occasional tourmaline uvite and schorl (Karimpour and Stern, 2010). In surface rocks, supergene argillic alteration overprints both QSCP and QCP altered rocks.

Some of the highest copper and gold grades are associated with the QSCP alteration zone (Cu 0.01–0.35 wt.%, Au < 0.1–2 ppm, Mo < 80 ppm, Zn < 100 ppm and Pb 10–200 ppm, in 56 samples). Pyrite, chalcopyrite

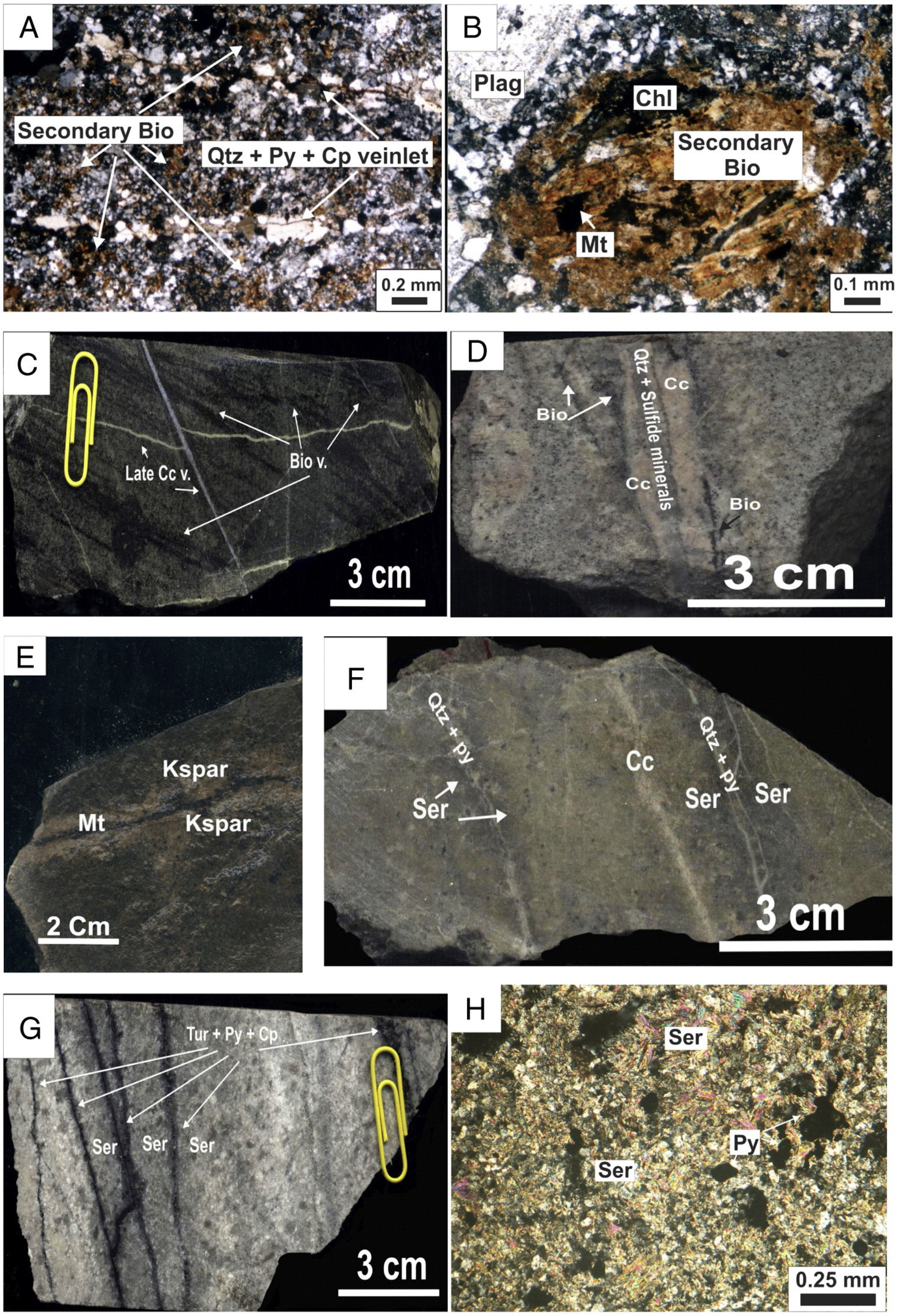

Fig. 14. Photomicrographs of hydrothermal alteration assemblages and mineralization from the Khopik prospect area. A. quartz-chalcopyrite-pyrite veinlet in potassic zone (KH–22 sample). B. Replacement of hornblende phenocryst by biotite, magnetite, and chlorite in potassic zone (KH–68 sample). C. Biotite veinlets crosscut by calcite veinlets (KH–18–B3). D. Quartz–calcite–chalcopyrite–bornite–biotite veinlet in potassic zone (KH–3–B3). E. Magnetite-biotite-K-feldspar-quartz veinlet in potassic zone (KH–24). F. Quartz-pyrite-sericite veinlets in QSCP zone (KH–14–B2). G. Tourmaline-pyrite-chalcopyrite veinlets in QSCP zone. (KH–50–B4). H. QSCP alteration (KH–50–B4 sample). I. Silicified alteration in dacitic-rhyodacitic tuffs (KH–6 sample). J. Hydrothermal breccia with QCP alteration (KH–19–B2). K. quartz-tourmaline-calcite-pyrite veinlets in QCP zone (KH–10–B1). L. Hydrothermal breccia showing the fine-grained, matrix-supported quartz-pyrite (KH–19–B2 sample). M. Propylitic alteration showing replacement of the magmatic hornblende by chlorite-calcite (KH–8–B1). N. Quartz-calcite-chlorite-sericite-chalcopyrite-pyrite veinlet in propylitic zone (KH–8–B1 sample). O. Propylitic alteration in hornblende diorite porphyry. Hornblende is replaced by chlorite, calcite, and magnetite (KH–110 sample–XPL). P. Enlargement of the previous photomicrograph (KH–110 sample). Qtz = Quartz, Py = Pyrite, Cp = Chalcopyrite, Bio = Biotite, Cc = Calcite, Kspar = K-feldspar, Mt = Magnetite, Ser = Sericite, Tur = Tourmaline, Chl = Chlorite, Hbl = Hornblende.

Please cite this article as: Malekzadeh Shafaroudi, A., et al., The Khopik porphyry copper prospect, Lut Block, Eastern Iran: Geology, alteration and mineralization, fluid inclusion, and oxygen isotope studies, Ore Geol. Rev. (2014), http://dx.doi.org/10.1016/j.oregeorev.2014.04.015

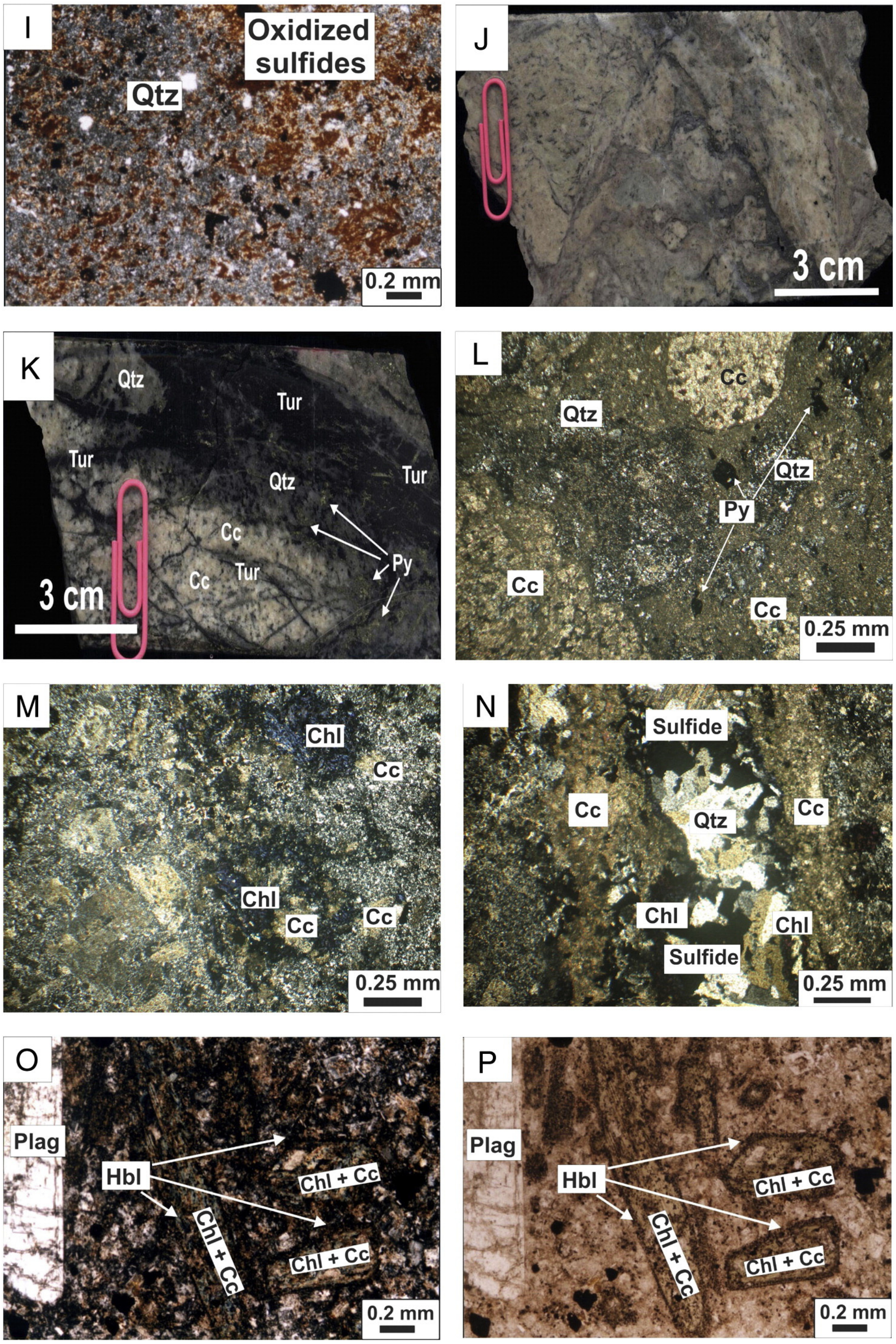

Fig. 14 (*continued*).

intergrown with minor bornite, and galena are the main sulfide minerals that occur with magnetite as disseminations and in stockworks. Massive mineralization is recognized in drill hole BH–01 in 211–216 m intervals and includes chalcopyrite (30%), tourmaline (15%), pyrite (~7%), magnetite (3–4%), quartz and calcite (Fig. 10A). The density of veinlets (0.1 mm–2 cm thick) in QSCP alteration zone is ≤ 4 veinlets/m^2 at the surface and ≤ 7/m^2 in drill holes (Figs. 9, 10A and B). Based on the mineralogy six types of veinlets are recognized in QSCP zone (Table 2), whereas quartz-carbonate-pyrite-chalcopyrite ± sericite veinlets are the most abundant. Pyrite is the earliest phase, chalcopyrite and bornite are slightly later, and galena is the latest formed sulfide mineral (Figs. 13 and 14F to H). The silicified zone, a subtype of QSCP alteration, mainly affected the andesites and dacitic to rhyodacitic tuffs in the western part of the Khopik prospect. The intensity of alteration is ≤ 50% (Fig. 9), and the mineral assemblage consists of quartz (□ 60%), pyrite, and tourmaline with minor calcite and sericite that replace plagioclase and K-feldspar. Less than 1% pyrite is recognized in silicified tuffs (see Fig. 14I).

Quartz-carbonate-pyrite (QCP) alteration is recognized in the hydrothermal breccia and locally in subvolcanic rocks, where it consists of quartz (≤30%), calcite (25–30%), pyrite (2–4%), and tourmaline

Please cite this article as: Malekzadeh Shafaroudi, A., et al., The Khopik porphyry copper prospect, Lut Block, Eastern Iran: Geology, alteration and mineralization, fluid inclusion, and oxygen isotope studies, Ore Geol. Rev. (2014), http://dx.doi.org/10.1016/j.oregeorev.2014.04.015

(□ 10%). Calcite and tourmaline commonly occur as veinlets and replacement zones. Stockwork, disseminated, and minor massive mineralization (□ 10% sulfides) dominantly consists of quartz with pyrite, chalcopyrite, bornite, and magnetite, as well as minor sphalerite occurring as intergrowths with chalcopyrite. The density of veinlets in QCP zone is < 25/m^2 in BH–01 at depths of 189.1–198.1 m (Fig. 10A).

Mineralogically, four types of veinlets (□ 1.5 cm wide) are recognized in QCP zone as described in Table 2. Quartz-carbonate-pyrite ± chalcopyrite ± tourmaline ± sphalerite veinlets are most abundant (Figs. 13 and 14J–L). No clear timing relationships could be established between these different veinlets, although the cross-cutting relationships suggest that quartz-carbonate-pyrite veinlets are older than carbonate-pyrite veinlets. Minor massive mineralization observed in BH–02 consists of magnetite, chalcopyrite, and pyrite, whereas sulfide and magnetite veinlets fill fractures of the massive magnetite. The Cu and Au contents are □ 0.2 wt. % and 0.1 ppm, respectively. Supergene argillic alteration overprints QSCP and QCP alteration zones where feldspars are replaced by clay minerals including kaolinite.

Quartz-carbonate alteration is a subtype of QCP alteration with no sulfides, and is only recognized at the western portion of the Khopik prospect. The alteration makes ≤ 50% of the rock's volume (Fig. 8) consisting of fine-grained (□ 50 μm) quartz aggregates with calcite partially replacing the hornblende and the plagioclase.

Propylitic alteration is very widespread (Fig. 10A) and affects the volcanic rocks and parts of the hornblende diorite porphyry, hornblende monzodiorite to monzonite porphyry, and monzonite porphyry. The alteration intensity is very variable reaching the highest intensity in the western part of the prospect (Fig. 8). It consists of quartz (30–35%), chlorite (□ 20%), epidote (□ 20% in volcanic rocks), calcite (□ 25%), and magnetite (□ 3%) with minor amounts of sericite and tourmaline. Mafic minerals and plagioclase were altered to chlorite, epidote, and calcite. Quartz occurs as veins, veinlets, microveins, and as interstitial fillings. Some mineralization formed in the propylitic alteration zone occurs as stockworks and as disseminations. The density of veinlets in propylitic alteration is < 5/m^2 and < 10 veinlets/m^2 on the surface and in drill holes, respectively (Figs. 8B, 9, and 10). Sulfide concentration is < 4%, although higher concentration of sulfide minerals (10–15%) occurs in the 269–278.5 m interval of the drill hole BH–04 (Fig. 10B). Pyrite, chalcopyrite, magnetite with minor bornite and sphalerite, locally intergrowth with chalcopyrite, are the main ore minerals.

Based on their mineralogy, seven types of veinlets (<3 mm wide) are recognized in this alteration type (Table 2 and Figs. 13 and 14M and P), at which pyrite-quartz-carbonate ± chalcopyrite ± chlorite ± sericite veinlets are most abundant. Metal concentrations in thirty two samples were Cu < 0.2 wt. %, Au < 0.1–0.3 ppm, Mo < 40 ppm, Zn 20–474 ppm, and Pb < 100 ppm.

Hydrothermal breccia consists of fragments of quartz-sulfide veinlets and intensely QSCP altered intrusions in a matrix of quartz, calcite, pyrite, and minor chalcopyrite. Three mineralization stages are recognized in hydrothermal breccias based on the three types of pyrite as described below:

1) Pyrite (<3%) within breccia fragments indicating pyrite formation prior to brecciation,
2) Pyrite-quartz assemblage as breccia matrix indicating that pyrite (2%, along with 0.5% chalcopyrite) was formed during hydrothermal brecciation,
3) Pyrite-calcite veinlets (10%) that formed after the brecciation stage (Fig. 10A and B).

Vein-type mineralization formed late along NNW-trending faults (~N 30°) that are mainly found in the eastern part of the prospect. Sulfides in these veins consist of pyrite, chalcopyrite, minor sphalerite and galena. Metal concentrations in 27 samples within the veins are Cu < 0.1–0.3%, Au < 0.1–1.2 ppm, Mo < 70 ppm, Zn < 100 and locally < 2500 ppm, and Pb < 50 ppm and locally < 500 ppm. Four types of fault-related veins and veinlets are recognized: 1) quartz-pyrite ± sphalerite ± galena ± arsenopyrite, 2) quartz-pyrite-chalcopyrite, 3) quartz-pyrite-tourmaline-sericite, and 4) quartz-carbonate-pyrite (Figs. 9 and 13) with the first two being the most abundant. The total content of sulfide minerals in these veins (<10 cm wide) is 8–10% with 2–3% pyrite, 6–8% chalcopyrite, and sphalerite and galena (0.5%) that occasionally occur in veinlets type-1.

7. Fluid inclusion data

7.1. Fluid inclusion petrography

Heating and freezing tests were made on primary fluid inclusions in quartz within UST layers, and in veins and veinlets of potassic and QSCP alteration zones. Care was taken to document the alteration or veinlet-filling mineral with which a given primary inclusion assemblage was associated. Secondary fluid inclusions were commonly readily distinguished under low power magnification in clearly defined planes which cut across, or terminated at, grain boundaries. Primary fluid inclusions were searched for in areas where secondary planes were not abundant, and were distinguished on the basis of criteria given by Roedder (1984). These key attributes used to determine primary fluid inclusions were: (1) isolation from other inclusions, (2) random distribution of inclusions (not on planar features), and (3) inclusions that typically follow growth zones and maybe associated with solid inclusions in host minerals.

Fluid inclusions were classified using the criteria given by Nash (1976). The less abundant fluid inclusions observed were < 5 μm in diameter and contained liquid plus a vapor bubble (LV), which occupied 20–50% of the inclusion volume (type–I). (LV) inclusions homogenized to the liquid by disappearance of the vapor bubble upon heating. Vapor-rich, two-phase inclusions (□ 10 μm in diameter) with a large vapor bubble (VL, Type–II) were observed in all samples of the studied veinlets (Fig. 15), and homogenized to vapor upon heating. The most abundant and largest fluid inclusions (6–42 μm in diameter) contained a halite cube at room temperature and a small to medium size vapor bubble (LVS), both of which dissolved upon heating (type–III). At least one other daughter crystal was usually present with the halite, but as many as three were observed in a single type–III inclusion (Fig. 15). The phases tentatively identified as hematite, pyrite, chalcopyrite, and anhydrite, as well as unidentified silicate minerals. The homogenization temperature for type–III inclusions is defined as the temperature at which the reminded last phase (vapor bubble or halite) had disappeared.

7.2. Microthermometry of fluid inclusions

During the course of this study, 108 homogenization temperatures and melting points of fluid inclusions were recorded. Four types of quartz-sulfide veinlets of potassic alteration (quartz-chalcopyrite-biotite-magnetite, quartz-magnetite-K-feldspar-pyrite-chalcopyrite, quartz-pyrite-chalcopyrite-magnetite, and quartz-pyrite-chalcopyrite ± K-feldspar) and quartz-chalcopyrite-pyrite-sericite veinlet of QSCP zone were analyzed. Results of microthermometric measurements are listed in Table 3. Homogenization temperatures of primary type–III (LVS) and type–II (VL) fluid inclusions from quartz in UST layers and four veinlets of potassic and one veinlet of QSCP alteration zones are shown in Fig. 16.

Vapor bubble disappeared from 455 to > 600 ºC (average 526 ºC in 33 runs) and 410–567 ºC (average 476 ºC in 41 runs) in type–III fluid inclusions in quartz of the UST and veinlets of potassic alteration, respectively. The temperature of the bubble disappearance decreased to 322 –380 ºC (average 348 ºC, n = 10) in quartz-chalcopyrite-pyrite-sericite veinlet of QSCP zone (Table 3; Fig. 16A). Salinities of type–III inclusions are estimated by halite dissolution temperatures, which are identical to homogenization temperature, if salt dissolution occurs after disappearance of the vapor bubble. Halite dissolved from 482 to > 600 ºC (average 546 ºC, n = 33) and 432–592 ºC (average 504 ºC, n = 41) in type–III fluid

Please cite this article as: Malekzadeh Shafaroudi, A., et al., The Khopik porphyry copper prospect, Lut Block, Eastern Iran: Geology, alteration and mineralization, fluid inclusion, and oxygen isotope studies, Ore Geol. Rev. (2014), http://dx.doi.org/10.1016/j.oregeorev.2014.04.015

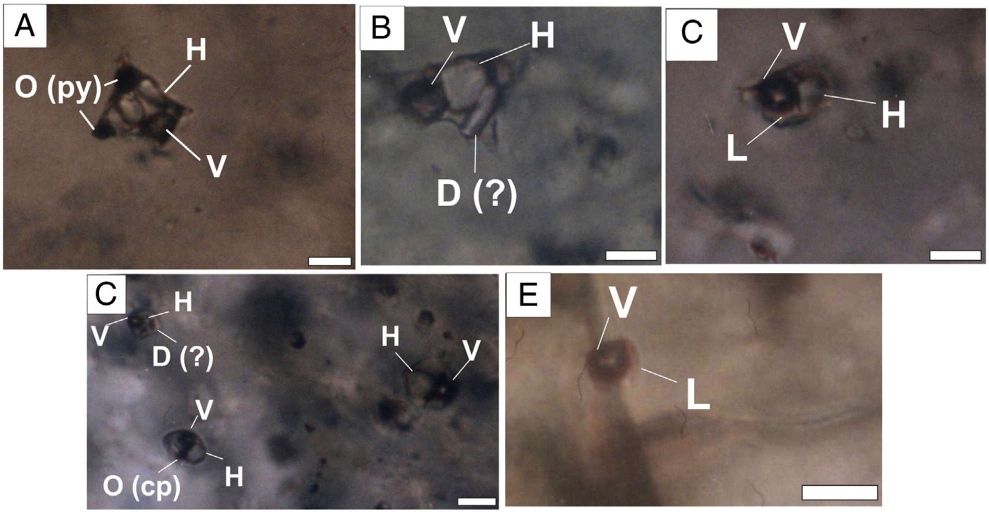

Fig. 15. Photomicrographs of primary fluid inclusions in quartz from UST layers and veinlets of potassic and QSCP alteration. A. Type–III inclusion in quartz-pyrite-chalcopyrite-magnetite veinlet of potassic zone (KH–36 sample–). B. Type–III inclusion in UST quartz (KH–85 sample). C. Type–III inclusion in quartz-magnetite-K-feldspar-pyrite-chalcopyrite veinlet of potassic zone (KH–64 sample). D. Type–III inclusions in quartz-chalcopyrite-pyrite-sericite veinlet of QSCP zone (KH–53 sample). E. Type–II inclusion in quartz-chalcopyrite-pyrite-sericite veinlet of QSCP alteration (KH–53 sample). Scale line under photomicrographs is 10 μm. L = Liquid, V = Vapor, H = Halite, O = Opaque daughter minerals, D = Daughter minerals (transparent), Py = Pyrite, Cp = Chalcopyrite.

inclusions in quartz of UST and veinlets of potassic alteration, respectively, whereas this temperature decreased to from 332–400 ºC (average 366 ºC, n = 10) in quartz-chalcopyrite-pyrite-sericite veinlet of QSCP zone (Table 3; Fig. 16B). These halite dissolution temperatures corresponded to salinities of 57.3 –74 wt. % NaCl equiv. (average 66.3 wt. % NaCl equiv., n = 33) and 51–72.8 wt. % NaCl equiv. (average 60.4 wt. % NaCl equivalent, n = 41) in type–III fluid inclusions in quartz of UST and veinlets of potassic alteration, respectively, whereas salinity decreased from 40.7–47.4 wt. % NaCl equiv. (average 44 wt. % NaCl equiv., n = 10) in quartz-chalcopyrite-pyrite-sericite veinlet of QSCP zone (Table 3; Fig. 16C).

The first melting temperatures (T_{fm}) values of type–III inclusions between –55 and –50.5 ºC (average –53.6 ºC, n = 25). Comparison of the values to the eutectic temperatures of various water-salt systems (Gokce, 2000; Shepherd et al., 1985) suggests that the hydrothermal fluids mainly contained $CaCl_2$-NaCl-H_2O ± other salts. Therefore, the total salinity of the halite-bearing inclusions determined by dissolution may be somewhat higher owing to an unknown salt content. The curvilinear distribution of the majority of type–III inclusions in Fig. 17 corresponds to the thermal dissolution curve of halite and results from the fact that all of these inclusions homogenized by halite dissolution.

A few heating and freezing analyses of type–II fluid inclusions could be measured in two samples of both UST layers and veinlets of potassic alteration. Homogenization temperatures of type–II inclusions range from 489 to > 600 ºC (average 547 ºC, n = 13) in UST layers and 437–531 ºC (average 487 ºC, n = 11) in veinlets of potassic alteration (Table. 3; Fig. 16D). The T_{fm} values of primary type–II inclusions in both UST layers and veinlets of potassic are between –55 and –50.5 ºC (average –53.6 ºC, n = 24). Comparison of the values to the eutectic temperatures of various water-salt systems (Gokce, 2000; Shepherd et al., 1985) suggests that the hydrothermal fluids contained $CaCl_2$-NaCl ± other salts. The last ice melting temperatures (T_m) range from –2.7 to –19.2 ºC

Table 3
Primary fluid inclusions microthermometry results from quartz of UST layers and quartz-sulfide veinlets of potassic and QSCP alteration zones from the Khopik prospect.

Type of sample	Inclusion type[9]	T_h^{10} (L-V) (°C)	T_s^{11} (NaCl) (°C)	T_m^{12} (°C)	Salinity (wt. % NaCl equiv.)
Potassic alteration					
UST layers[1]	III	455 to >600	494 to >600	–	59–73.9
	II	502 to >600	–	–2.7 to –19.2	4.4–21.8
UST layers [2]	III	463 to >600	482 to >600	–	57.3–73.9
UST layers [3]	III	472–583	489–592	–	58.2–72.8
	II	489 to >600	–	–6.3 to –17.2	9.6–20.4
Qtz-Cp-Py-Mt veinlet[4]	III	410–567	432–592	–	51–72.8
	II	479–531	–	–7.8 to –15.3	11.5–18.9
Qtz-Mt-Kspar-Py-Cp veinlet[5]	III	432–522	452–541	–	53.5–65.4
Qtz-Py-Cp-Mt veinlet[6]	III	423–500	472–542	–	56–65.6
Qtz-Py-Cp ± Kspar veinlet[7]	III	415–495	442–535	–	52.2–64.6
	II	437–504	–	–9.7 to –12.7	13.6–16.6
Quartz–sericite–carbonate–pyrite alteration					
Qtz–Cp–Py–Ser veinlet[8]	III	322–380	332–400	–	40.7–47.4

Abbreviations: Qtz = Quartz, Py = Pyrite, Cp = Chalcopyrite, Kspar = K-feldspar, Mt = Magnetite, and Ser = Sericite.
1- KH-85 sample (684148E, 3582756 N), 2- KH-86 sample (684125E, 3582747 N), 3- KH-87 sample (684116E, 3582734 N), 4- KH-28 sample (685719E, 3581819 N), 5- KH-64 sample (684764E, 3582280 N), 6- KH-36 sample (685682E, 3581827 N), 7- KH-81 sample (684145E, 3582725 N), and 8- KH-53 sample (685573E, 3582226 N).
9- See Table 3.
10- T_h = temperature of vapor bubble disappearance in type–III fluid inclusions and vapor expansion in type–II fluid inclusions.
11- T_s = temperature of halite dissolution in type–III fluid inclusions.
12- T_m = final temperature of ice melting.

Please cite this article as: Malekzadeh Shafaroudi, A., et al., The Khopik porphyry copper prospect, Lut Block, Eastern Iran: Geology, alteration and mineralization, fluid inclusion, and oxygen isotope studies, Ore Geol. Rev. (2014), http://dx.doi.org/10.1016/j.oregeorev.2014.04.015

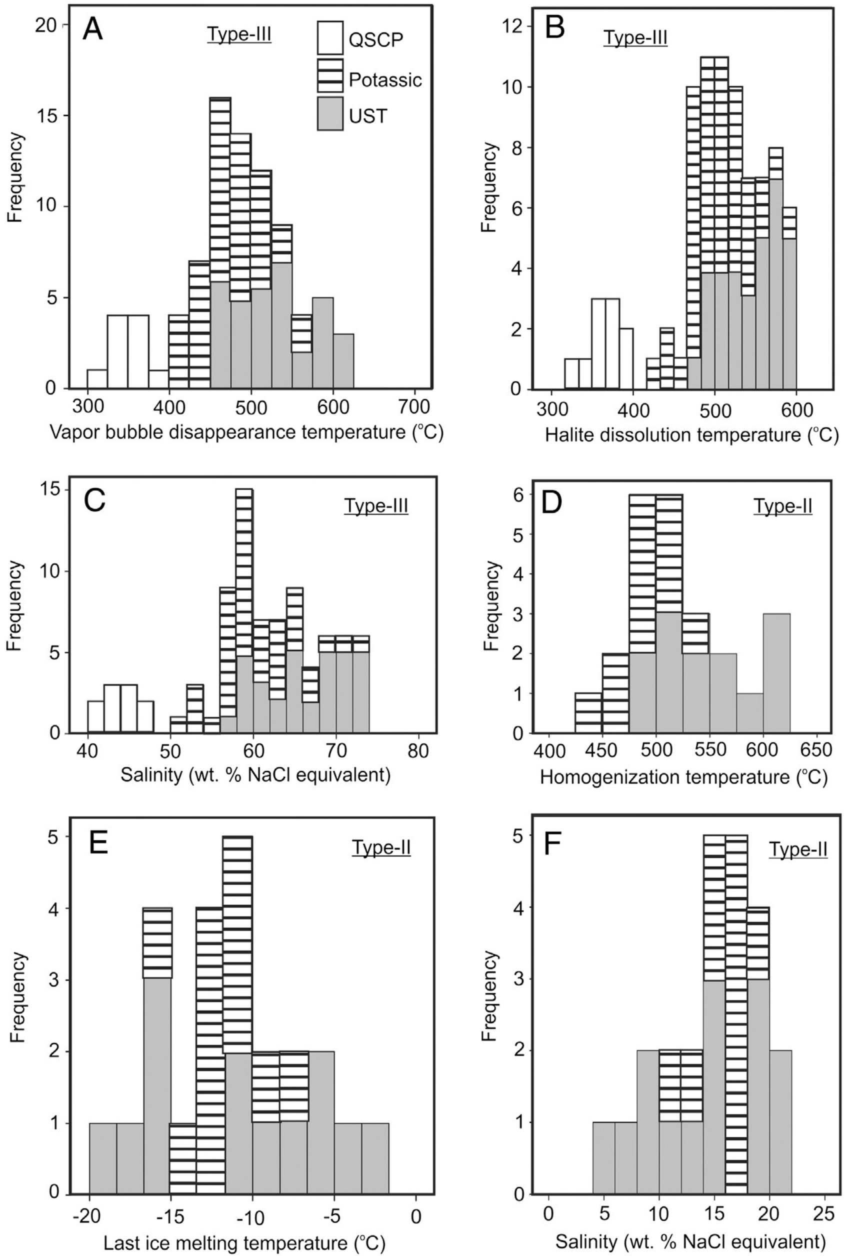

Fig. 16. Histograms showing plots of microthermometric data for the type–III and type–II fluid inclusions of UST quartz and veinlets of potassic and QSCP alterations: A. Vapor bubble disappearance temperature of type–III fluid inclusions. B. Halite dissolution temperature of type–III fluid inclusions. C. Salinity of type–III fluid inclusions. D. Homogenization temperature of type–II fluid inclusions. E. Last ice melting temperature of type–II fluid inclusions. F. Salinity of type–II fluid inclusions.

(average −10.9 ºC, n = 13) in UST layers and −7.8 to −15.3 ºC (average −11.7 ºC, n = 11) in veinlets of potassic alteration (Table 3; Fig. 16E). The salinities of the hydrothermal fluids were calculated using the equation of Bodnar (1993), and yielded wt. % NaCl equiv. as follows: 4.4–21.8 wt. % NaCl equiv. (average 14.3 wt. % NaCl equiv., n = 13) in UST layers and 11.5–18.9 wt. % NaCl equiv. (average 15.6 wt. % NaCl equiv., n = 11) in veinlets of potassic alteration (Table 3; Fig. 16 F). The obvious changes in fluid characteristics for the samples studied is the shift from high temperatures and high salinities in UST layers and early veinlets at potassic alteration to predominance of moderate temperatures and salinity fluids in later veinlet at QSCP alteration zone (Fig. 17).

A pressure correction is necessary to convert the homogenization temperatures to true trapping temperatures. A few scattered groups of coexisting type–I (LV) and type–II (VL) inclusions were seen in the study samples, but the homogenization temperatures of the type–I inclusions were not measured to can integrate the results in the discussion in regard with boiling. However, homogenization temperature and salinity data for the primary inclusions coupled with lack of evidence for boiling enable a lower limit to be placed on pressure at approximately 448 bars at 482 ºC to > 1000 bars at > 600 ºC, 400 bars at 432 ºC to 743 bars at 592 ºC, and 114 bars at 332 ºC to 260 bars at 400 ºC in the UST layers, veinlets of potassic alteration, and veinlets of QSCP alteration, respectively (HOKIEFLINCS-H2O-NACL program, Lecumberri-Sanchez et al., 2012; Steele-MacInnis et al., 2012).

A pressure of 114 bars represents a minimum depth of burial of slightly near 1 km if confining pressure were lithostatic; extrapolation of data given by Hass (1971) for a continuously boiling column of 40 weight percent NaCl solution provides a minimum hydrostatic depth of burial equal to about 3 km. No confident estimates are available for the thickness of the rock column originally overlying the Khopik deposit. Owing to the lack of information concerning pressures of formation of all of the veins studied, homogenization temperatures of most fluid inclusions analyzed

Please cite this article as: Malekzadeh Shafaroudi, A., et al., The Khopik porphyry copper prospect, Lut Block, Eastern Iran: Geology, alteration and mineralization, fluid inclusion, and oxygen isotope studies, Ore Geol. Rev. (2014), http://dx.doi.org/10.1016/j.oregeorev.2014.04.015

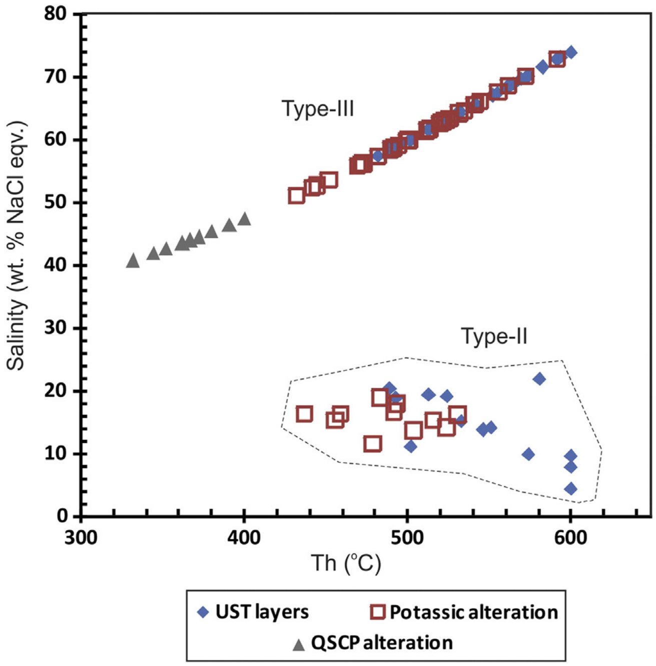

Fig. 17. Homogenization temperatures and salinities of type–III and type–II fluid inclusions from all studied samples. The highest salinities correspond to the estimated salinities for inclusions homogenizing by halite dissolution.

cannot be confidently converted to temperatures of trapping (i.e., formation temperatures). However, the data gathered for fluid inclusions can be interpreted to indicate that the variations observed in homogenization temperatures reflect corresponding changes in fluid trapping temperatures.

8. Oxygen Isotope Studies

Three quartz samples from UST, two quartz samples from veinlets of potassic alteration, and one sample of quartz in a quartz-chalcopyrite-pyrite-sericite veinlet from QSCP alteration were used for oxygen isotope studies. The δ^{18}O values of the quartz samples vary from 11.1–12.7 ‰ relative to Standard Mean Ocean Water (SMOW) with a mean of 11.7 ‰ (Table 4) and are similar to those of magmatic rocks (see Hoefs, 1984). These results may suggest a magmatic source. The relatively narrow range of the δ^{18}O values suggests that the isotopic character of the ore-forming fluids did not significantly change temporally and spatially during the episode of quartz veinlet formation. The δ^{18}O values for water in equilibrium with quartz were estimated using the equation of Hu and Clayton (2003) and Zhang et al. (1989) and the homogenization temperature values obtained during our fluid inclusion studies. These calculated δ^{18}O values vary in a narrow range from +7.3 to +9.3 ‰ (SMOW). The $\delta^{18}O_{water}$ composition of the UST ranges from 8.7–8.9 ‰. Quartz in quartz-pyrite-chalcopyrite-magnetite and quartz-magnetite-K-feldspar-pyrite-chalcopyrite veinlets of the potassic zone has similar calculated $\delta^{18}O_{water}$ values of 9.0 and 9.3‰, respectively, and the $\delta^{18}O_{water}$ value in a quartz-chalcopyrite-pyrite-sericite veinlet of the QSCP alteration is estimated as 7.3 ‰ (Table 4).

The results plot in the magmatic water field on the $\delta^{18}O_{water}$ versus homogenization temperature diagram, which indicates that the ore-forming fluids isotopically possessed dominantly magmatic characteristics during the formation of the UST layers and quartz veinlets (Fig. 18).

9. Discussion

9.1. Nature of the ore fluids

The +7.3 to +9.3 ‰ calculated δ^{18}O values of the fluids in UST layers and veinlets of potassic and QSCP alteration zones strongly support their formation from magmatic waters within the temperature range of 300–600 ºC as obtained from the fluid inclusion studies. Since the sulfides are in general intimately associated with the quartz veinlets at Khopik prospect, it can be further inferred that the ore sulfides were also primarily deposited by these fluids.

The lowest $\delta^{18}O_{water}$ value of +7.3 ‰ is recorded from a sample taken from quartz-chalcopyrite-pyrite-sericite veinlet of the QSCP alteration with lowest homogenization temperatures (322–380 ºC) and salinities (40.7–47.4 wt. % NaCl equiv.). Admixture of magmatic fluids with the dominant meteoric waters is considered to produce sericitic alteration and the low- to moderate-salinity fluid, i.e., 5–10× dilution of the hypersaline liquid (e.g., Sheppard et al., 1971; Taylor, 1974). Recent interpretations of the stable O and H isotope data reveal that an exclusively magmatic fluid is quite capable of producing the chlorite-sericite and sericitic assemblages (Harris and Golding, 2002; Hedenquist and Richards, 1998; Hedenquist et al., 1998; Khashgerel et al.,

Table 4
Oxygen isotope data from UST layers and veins and veinlets of potassic and QSCP alteration zones.

Sample No., and Location	Type of sample	$\delta^{18}O_{quartz}$ (‰)	T_{mean} (°C) fluid calculated	1000 lnα (Hu and Clayton, 2003)	$\delta^{18}O_{water}$ ‰))
KH-87 684116E 3582734 N	UST	11.25	544	2.36	8.9
KH-85 684148E 3582756 N	UST	11.09	551	2.30	8.8
KH-86 684125E 3582747 N	UST	11.13	539	2.40	8.7
KH-64 684764E 3582280 N	Qtz-Py-Cp-Mt veinlet of potassic alteration zone	11.83	497	2.80	9.0
KH-36 685682E 3581827 N	Qtz-Mt-Kspar-Py-Cp veinlet of potassic alteration zone	12.08	497	2.80	9.3
KH-–53 685973E 3582347 N	Qtz-Cp-Py-Ser veinlet of QSCP alteration zone	12.70	366	5.38*	7.3

NOTES: abbreviations - Qtz = Quartz, Py = Pyrite, Cp = Chalcopyrite, Kspar = K-feldspar, Mt = Magnetite, and Ser = Sericite.
* Zhang et al. (1989).

Please cite this article as: Malekzadeh Shafaroudi, A., et al., The Khopik porphyry copper prospect, Lut Block, Eastern Iran: Geology, alteration and mineralization, fluid inclusion, and oxygen isotope studies, Ore Geol. Rev. (2014), http://dx.doi.org/10.1016/j.oregeorev.2014.04.015

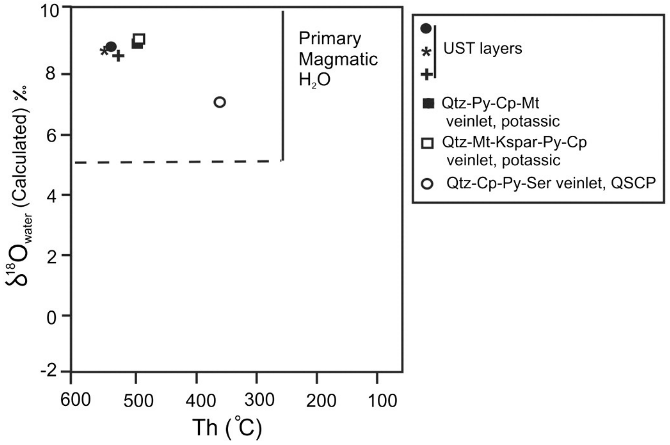

Fig. 18. $\delta^{18}O_{water}$ versus homogenization temperature diagram with the field of primary magmatic water of Sheppard (1986). All Khopik samples plot in the magmatic water filed.

2006; Kusakabe et al., 1990; Rusk et al., 2004; Skewes et al., 2003; Watanabe and Hedenquist, 2001); however, late convecting meteoric water may still be responsible for some sericitic alteration, along the perimeter of advecting magmatic volatiles (see Beane and Titley, 1981; Hunt, 1991). Meteoric water can equilibrate at high temperatures with igneous rocks affecting isotopic exchange with silicates. This results in increases in $\delta^{18}O$ and δD values in modified meteoric waters to the range of magmatic waters; this depends on initial isotopic values in both the water and rock, the fluid-rock ratio, and the reaction temperatures. Therefore, it can be conceived that the ore-forming fluids at Khopik could have been: (1) predominantly magmatic water and/or (2) a mixture of magmatic and meteoric water. It is crucial to note that the single sample from QSCP alteration zone might not be representative for the formation of all of the veinlets in this zone, and should not be generalized for the overall history of the fluid evolution at Khopik.

Our fluid inclusion studies indicate that quartz from UST layers and veinlets of potassic alteration crystallized from a two-phase fluid consisting of a hypersaline liquid (brine; type–III, LVS) and a low density vapor-rich (type–II, VL) phase. Coexistence of immiscible hypersaline liquid and vapor has been demonstrated in numerous fluid inclusion studies (Roedder, 1984, 1992). Enrichment in Na, K, and Fe chlorides gives rise to salinities of 35–70 wt. % NaCl equiv. (e.g. Bodnar, 1995; Eastoe, 1978; Nash, 1976), whereas the vapor phase contains volatile species, predominantly SO_2, CO_2, and HCl (e.g., Giggenbach, 1997). The association of halite-saturated fluid inclusions (type–III) with vapor-rich inclusions (type–II) in veinlets of potassic alteration zones is typical of fluid inclusion assemblages in porphyry copper deposits formed at shallow, ≤4 km depths (Beane and Bodnar, 1995; Bodnar, 1995; Sillitoe, 2010). At these depths, the mineralization is introduced by a two-phase fluid, comprising a small fraction of hypersaline liquid (brine) and a much larger volume of low-density vapor (Fournier, 1999), produced by either direct exsolution from the melt (Shinohara, 1994) or, more typically, as the single-phase liquid decompresses, cools, and intersects its solvus (e.g., Bodnar, 1995; Cline, 1995; Henley and McNabb, 1978; Webster, 1992).

Fluid inclusion data indicate that the ore-forming fluids contain significant quantities of $CaCl_2$ and NaCl ± other salts. Halite dissolution temperatures in quartz decrease from UST layers (482 to > 600 °C) to veinlets in QSCP alteration zones (332–400 °C) coincidently with a decrease of salinity from 57.3–73.9 wt. % NaCl equiv. in UST layers to 40.7–47.4 wt. % NaCl equiv. in veinlet of QSCP alteration zone indicating an evolving ore fluid (Fig. 17). Accordingly, the homogenization temperatures and salinities of vapor-rich (type–II) inclusions range from 489–600 ºC with 4.4–21.8 wt. % NaCl equiv. in UST layers, and 437–531 ºC with 11.5–18.9 wt. % NaCl equiv. in veinlets of potassic alteration. As with other porphyry copper systems (e. g., Heinrich, 2005; Williams-Jones and Heinrich, 2005), phase separation between vapor and hypersaline liquid could have initiated concentration of Cu and Au (and Mo) at Khopik. Likewise, potassic alteration was probably also initiated through cooling at 700–550 °C temperature range, in and around the early porphyry stocks, perhaps together with the first metal precipitation as evidenced in other cases a. o., by Bodnar (1995), Frei (1995), and Ulrich et al. (2001).

9.2. Mineralization model

Porphyry Cu systems typically span the upper 4 km or so of the crust (Singer et al., 2008), with their centrally located stocks being connected downward to parental magma chambers at depths of perhaps 5–15 km (Cloos, 2001; Richards, 2005). The parental chambers, tending to be localized at sites of neutral buoyancy (Cloos, 2001; Richards, 2005), are the sources of both magmas, and high-temperature, high-pressure metalliferous fluids throughout system development.

The shallow-level porphyry stocks do not themselves generate the bulk of the magmatic fluid volume, but simply act as "exhaust valves," conduits for its upward transmission from the parental chambers, perhaps via cupolas on their roofs. This scenario implies episodic but focused magma and fluid ascent for as long as ~5 Ma in the case of long-lived porphyry Cu systems, whereas elsewhere the loci of intrusive and hydrothermal activity migrate, either systematically or randomly, to give rise to the porphyry Cu and epithermal Au deposit clusters and alignments discussed above (Sillitoe, 2010).

Cloos (2001) suggested that porphyry copper deposits can form when H_2O-unsaturated magma is emplaced into wall rock that is cool enough that steep lateral thermal gradients create a narrow solidification front. At depths less than ~4 km, cooling and crystallization cause fluid saturation to occur within sidewall magma that is mobile because it contains less than ~25% suspended crystals. After a sufficient volume of bubbles forms, mobile sidewall magma buoyantly rises instead of sinking. The bubbles expand as they decompress, and at depths of ~2 km they become large enough to rise on their own, separate from the upwelled magma, and charge the cupola at the top of the stock with magmatic fluid. The partially degassed magma sinks into the interior of the stock. Upwelling of saturated sidewall magma entrains deeper-seated, nearly saturated magma, which decompresses and saturates as it rises. As the system cools, the depth of H_2O saturation and sidewall upwelling increases. Bubbles of copper-rich fluid are generated where the saturation front extends to depths of ~6 km or more. Overall, the system is cooling, but the upward advection of heat maintains the cupola region at roughly constant position for the life of convective upwelling along the sidewalls. Porphyry copper ore deposits can form where draining of the fluid pocket beneath a cupola is steady and a large volume of magma is cycled through the system. Magma in the stock that escapes to intrude commonly has a porphyritic texture because crystal growth is enhanced, and nucleation is suppressed when the magma is H_2O saturated (Cloos, 2001).

Copper-gold mineralization at the Khopik prospect is spatially and temporally associated with subvolcanic calc-alkaline oxidized rocks (Fig. 19A). Crystallization of the monzonite stocks took place over a short time span during the Middle Eocene (39.0 ± 0.8 Ma to 38.2 ± 0.8 Ma). The earliest stage of mineralization was related to the emplacement of the hornblende quartz monzonite and is associated with weak potassic alteration and sub-economic pyrite-chalcopyrite mineralization in widely spaced quartz stockwork veins and veinlets.

The most important stage of veining in the Khopik is related to the emplacement of biotite-hornblende quartz monzodiorite to monzonite porphyry that is spatially associated with potassic alteration assemblages. The presence of hornblende and biotite phenocrysts in biotite-hornblende quartz monzodiorite to monzonite porphyry is indicating high magmatic water contents.

Please cite this article as: Malekzadeh Shafaroudi, A., et al., The Khopik porphyry copper prospect, Lut Block, Eastern Iran: Geology, alteration and mineralization, fluid inclusion, and oxygen isotope studies, Ore Geol. Rev. (2014), http://dx.doi.org/10.1016/j.oregeorev.2014.04.015

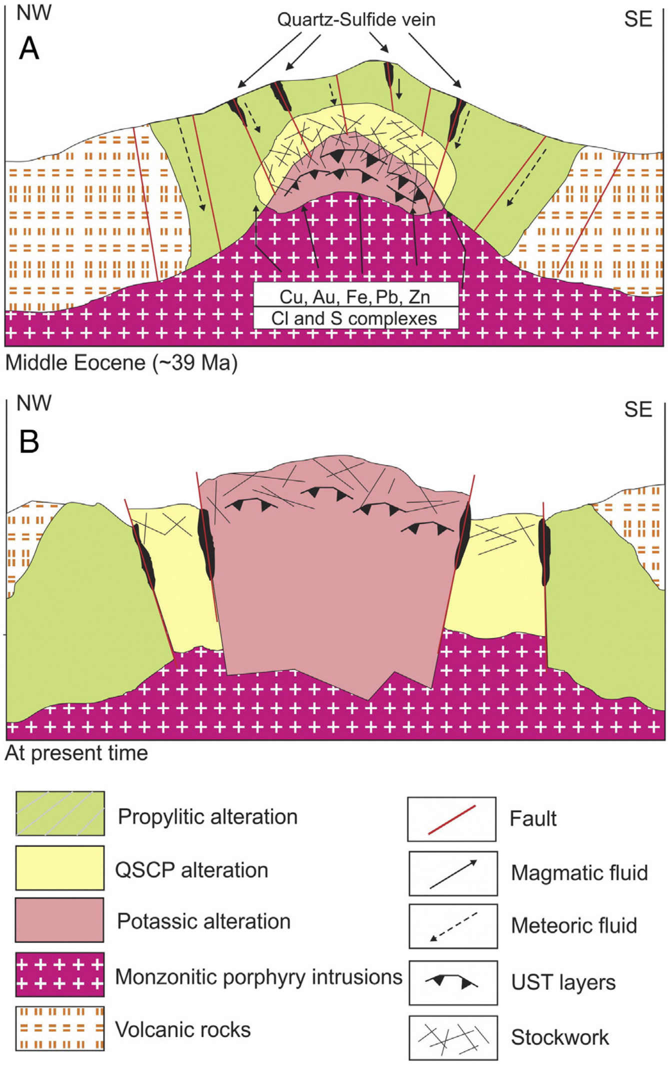

Fig. 19. A. Schematic model for formation of the Khopik deposit with UST layers and veinlets of potassic and QSCP alteration zones. B. Uplifting of intrusions, extensive erosion, and exposure of potassic and QSCP alteration zones and high density of veinlets at surface (not to scale).

Exsolution of magmatic water and migration towards the upper parts of the intrusive bodies represents a necessary step in porphyry copper genesis, involving the release of magmatic-hydrothermal volatiles from a crystallizing porphyritic intrusion (Dilles, 1987). According to Burnham and Ohmoto (1980) and Burnham (1985), fluids accumulate beneath the carapace of the crystallizing stock at a depth of ~3.5 km leading to carapace failure, pressure decrease, and a second boiling event. This happens when fluid pressure exceeds the lithostatic pressure and rupture of the carapace. The hydrofracturing initially lead to increased volatile exsolution from the magma, however fractures subsequently sealed due to mineral deposition and/or lithostatic compression. Pressure cycling then resulted in multiple fracture events (Dilles and Einaudi, 1992; Gustafson and Hunt, 1975). This process was repeated several times and likely played an important role in forming UST layers and different type of veinlets at the Khopik system. Potassic alteration with intense quartz-sulfide (pyrite, chalcopyrite, bornite, sphalerite) ± magnetite veining (Dilles and Einaudi, 1992; Gustafson and Hunt, 1975), typical of most economic porphyry copper deposits, is closely linked with the emplacement of the biotite-hornblende quartz monzodiorite to monzonite porphyry at Khopik (Fig. 19A). The associated mineralization probably represents the main phase of Cu and Au introduction at the Khopik. Potassic alteration and associated metal deposition are initiated under near-lithostatic conditions and involve extensive hydraulic fracturing of the ductile rock at high strain rates (Fournier, 1999) to generate the pervasive stockwork veining.

In the later stage, hornblende monzodiorite to monzonite porphyry and monzonite porphyry were emplaced. They were mainly affected by QSCP to QCP and propylitic alteration. Some portions of quartz-sulfide ± magnetite ± other gangue minerals stockwork veinlets formed at this stage. Sericitic alteration in porphyry Cu deposits normally overprints and wholly or partially destroys the potassic and chlorite-sericite assemblages. This alteration is commonly pyrite dominated, implying effective removal of the Cu (±Au) present in the former chlorite-sericite and/or potassic assemblages (Sillitoe, 2010).

During the later stage, hydrothermal breccia overprinted the subvolcanic porphyries and sulfide mineralization. Magmatic-hydrothermal brecciation may be triggered by sudden release of fluid overpressures caused by roof failure above large, expanding vapor bubbles (Burnham, 1985; Norton and Cathles, 1973), particularly near the ductile-brittle transition (Fournier, 1999). Stockwork mineralization continued after the formation of hydrothermal breccias in the area, as indicated by quartz-sulfide veinlets that cut breccia clasts and the cement between them.

In the later stage, hornblende diorite porphyry was emplaced and associated with propylitic alteration and sub-economic pyrite-chalcopyrite mineralization manifested by widely spaced, quartz stockwork veinlets. Porphyritic stocks at the Khopik are mainly in fault contact with volcanic rocks. Parts of quartz-sulfide mineralization occur in fault zones as vein type mineralization associated with the latest stage of hydrothermal activity. These faults are reverse-type, which caused the uplift of mineralized monzonitic intrusive rocks. Extensive erosion exposed the potassic alteration, high grade Cu-Au, and the high density veinlets (Fig. 19B). Supergene oxidation of sulfide minerals formed the associated gossan zone with hematite, goethite, malachite, and argillic alteration.

9.3. Mineralization in Lut Block

The Lut Block is the main metallogenic province in east of Iran that comprises numerous porphyry Cu and Cu-Au prospects (Arjmandzadeh, 2011; Malekzadeh Shafaroudi, 2009; Malekzadeh Shafaroudi et al., 2009, 2010, 2012; Richards et al., 2012), low and high sulfidation epithermal Au deposits (Abdi and Karimpour, 2012; Arjmandzadeh et al., 2011), Cu-Pb-Zn vein-type deposits (Lotfi, 1982; Malekzadeh Shafaroudi and Karimpour, 2013a,b; Mehrabi et al., 2011; Mirzaee et al., 2012), probably some iron oxide copper-gold (IOCG) deposits as suggested by Karimpour et al. (2005), Sn vein-type (Esmaeily et al., 2005), polymetallic (Sn-Au-Cu-As-Pb-Zn) vein-type deposits (Hamoni et al., 2013; Karimpour et al., 2013), and intrusion-related gold systems (Karimpour et al., 2007). A few types of mineralization, such as Sn vein-type and polymetallic (Sn-Au-Cu-As-Pb-Zn) vein-type deposits, are related to Jurassic and Cretaceous S-type granitic intrusions resulting from microcontinental collision in the Lut Block, whereas the most mineralization occurred in the Tertiary due to its past subduction zone tectonic setting between the Lut and the Afghan Blocks, which led to extensive arc-related magmatic activity (Karimpour et al., 2012). Tertiary intrusive granitoids (related to mineralization) within the Lut Block in the province of Khorasan Razavi and South Khorasan are mainly subvolcanic with porphyry texture and their composition changes between granite to diorite, but monzonite is dominant. They are classified as belonging to the magnetite-series of I-type granitoids, with the exception of the Hired area. Chemically, they are metaluminous and K-rich and plot in the field of calc-alkaline to adakite intrusions in a large-scale area (Karimpour et al., 2012).

Karimpour et al. (2012) studied the relationships between different types of mineralization and the Tertiary granitoid rocks (syn-mineralization units) in the Lut Block using Rb-Sr isotope, geochemistry, and the radiometric ages. The U-Pb zircon age (43.3–33.3 Ma) indicate a middle Eocene to lower Oligocene for the intrusions, and the initial

Please cite this article as: Malekzadeh Shafaroudi, A., et al., The Khopik porphyry copper prospect, Lut Block, Eastern Iran: Geology, alteration and mineralization, fluid inclusion, and oxygen isotope studies, Ore Geol. Rev. (2014), http://dx.doi.org/10.1016/j.oregeorev.2014.04.015

$^{87}Sr/^{86}Sr$ ratios varying from 0.7051–0.7047 indicates that the related magma originated from oceanic crust or modified suprasubduction zone mantle. Therefore, the period during which the formation of the ore minerals took place coincides with Middle Eocene to Lower Oligocene. This is referred to as the metallogenic epoch for the Lut Block.

Plate conversion and subduction associated with intrusion of large subvolcanic intrusions at early Cenozoic (Eocene-Oligocene) at the Lut Block offers a favorable region for the formation of porphyry copper and related epithermal gold deposits. Eastern Iran can potentially become the second important porphyry copper belt in Iran after the UDMB. Richards et al. (2012) compared porphyry-related suites with earlier barren volcanoplutonic rocks in eastern Iran and suggested the porphyry-related suites were relatively evolved and fractionated significant amounts of hornblende prior to plagioclase crystallization as a consequence of high magmatic water contents.

A comparison of the Khopik porphyry Cu-Au prospect with porphyry copper deposits of the UDMB indicates that the UDMB Miocene porphyry deposits formed during convergence of the Afro-Arabian plate with Central Iran (Richards et al., 2012). The exact timing of porphyry formation relative to final collision is unclear, but Shafiei et al. (2009) have suggested that the mid-Miocene porphyries are syncollisional and related to crustal thickening. They formed at a late stage in the development of the UDMB, following a major volcanic stage in the Eocene-Oligocene. Subsequently, postcollisional alkaline magmatism has characterized the Pliocene-Quaternary period (Richards et al., 2012). In addition, the copper mineralization in eastern Iran appears to be gold-rich, whereas copper deposits of the younger UDMB is in general not rich.

10. Conclusions

Based on geology, alteration styles, mineralization types, geochemistry, fluid inclusion, and oxygen isotope data, the Khopik prospect area belongs to the broad class of porphyry copper deposits. These characteristics can be summarized as follows:

(1) The Khopik porphyry Cu-Au deposit occurs in an area covered by Eocene calc-alkaline volcanic rocks and spatially and temporally related subvolcanic intrusive stocks exposed along northwest-southeast oriented trends in the eastern part of the Lut Block, eastern Iran. The ore-bearing porphyries range from magnetite-series monzonite to diorite with metaluminous I-type, and high-K calc-alkaline to shoshonitic arc-like intrusions. Their initial $^{87}Sr/^{86}Sr$ and $^{143}Nd/^{144}Nd$ ratios are considered as representative of oceanic slab derived magmas or possibly related suprasubduction zone lithospheric mantle. The presence of hornblende and biotite phenocrysts in syn-mineralization intrusions indicates high magmatic water (P_{H2O}) contents.

(2) Hydrothermal alteration includes potassic, sericitic-potassic, QSCP, QCP, and propylitic zones within host monzonitic intrusions. These types of mineralization occur as disseminated, stockwork, and minor hydrothermal breccia styles. In addition, some mineralization is localized along fault zones as quartz-sulfide veins systems superimposed onto the porphyry system. The main ore minerals are pyrite, chalcopyrite, bornite, and magnetite. Extensive erosion exposed the potassic alteration, high grade Cu-Au, and the stockwork vein network at surface.

(3) The $\delta^{18}O$ values of the quartz in UST layers and veinlets of potassic and QSCP alteration zones vary from 11.1–12.7‰. Calculated $\delta^{18}O$ values of H_2O in equilibrium with quartz are in the range of +7.3 to +9.3‰, falling within the range of magmatic waters.

(4) Fluid inclusion data indicate that the ore-forming fluids contain significant quantities of $CaCl_2$ with high NaCl contents. Quartz from UST layers and veinlets of potassic alteration crystallized from a two-phase fluid consisting of a hypersaline (LVS) brine (type–III) and a low density vapor-rich (type–II) phase. Halite dissolution temperatures, identical to homogenization temperature of type–III fluid inclusions, in quartz decreases from UST layers (482 to > 600 °C) and veinlets of potassic alteration (432–592 °C) to veinlet of QSCP alteration zones (332–400 °C) concomitantly with a decrease of salinity (57.3–73.9 wt. % NaCl equiv. to 51–72.8 wt. % NaCl equiv. and to 40.7–47.4 wt. % NaCl equiv. respectively, suggesting an evolving fluid. Homogenization temperatures and salinities of vapor-rich (type–II) phases range from 489–600 ºC with 4.4–21.8 wt. % NaCl equiv. in UST layers and 437–531 ºC with 11.5–18.9 wt. % NaCl equiv. in veinlets of potassic alteration.

(5) The formation of the Khopik porphyry Cu-Au deposit is related to Middle Eocene magmatic activity, resulting from subduction of the Afghan Block beneath the Lut Block in eastern Iran. Geology, alteration, mineralization, and petrogenesis of these intrusions should be considered in any further exploration in the Lut Block.

(6) This episode of middle Eocene to lower Oliocene magmatism and mineralization was widespread in eastern Iran, and is likely an important copper belt, second in Iran only to the Urumieh-Dokhtar copper belt.

Subduction associated with intrusion of large high-K to shoshonitic subvolcanic intrusions at early Cenozoic (Eocene-Oligocene) at the Lut Block offers a favorable region for formation of gold-rich porphyry copper and related epithermal gold deposits. The many witnesses of these deposits observed in different places of the Lut Block need detailed works.

Acknowledgments

Our thanks are due to W. Atkinson and L. Farmer (University of Colorado, USA) for their constructive comments on the first version of the manuscript, and to T. Vennemann (University of Lausanne, Switzerland) for providing the stable isotope data. We thank J. Walther (Karlsruhe Institute of Technology-KIT, Germany) and J. Dilles (Oregon State University, USA) for further revisions, and the Pars Kaneh Company for access to the drill hole samples and the permission to publish the study results. This paper benefited from extensive editorial work and revisions by D. Lentz (University of New Brunswick, Canada) and F. Daliran (KIT, Germany).

References

Abdi, M., Karimpour, M.H., 2012. Geology, alteration, mineralization, petrogenesis, dating, geochemistry, and airborne geophysics of Kuh-Shah, SW Birjand. Iran. J. Econ. Geol. 4, 107–177 (in Persian with English abstract).

Ahmadian, J., Haschke, M., McDonald, I., Regelous, M., Ghorbani, M.R., Emami, M., Murata, M., 2009. High magmatic flux during Alpine-Himalayan collision: constraints from the Kal-e-Kafi complex, central Iran. Geol. Soc. Am. Bull. 121, 857–867.

Alavi, M., 1991. Tectonic map of the Middle East (1:5000,000): Tehran. Geological Survey of Iran.

Arjmandzadeh, R., 2011. Mineralization, geochemistry, geochronology, and determination of tectonomagmatic setting of intrusive rocks in Dehsalm and Chahshaljami prospect areas, Lut block, east of Iran. (PhD Thesis) Ferdowsi University of Mashhad (215 pp. (in Persian)).

Arjmandzadeh, R., Karimpour, M.H., Mazaheri, S.A., Santos, J.F., Medina, J.M., Homam, S.M. , 2011. Sr-Nd isotope geochemistry and petrogenesis of the Chah-Shaljami granitoids (Lut block, eastern Iran). J. Asian Earth Sci. 41, 283–296.

Beane, R.E., Bodnar, R.J., 1995. Hydrothermal fluids and hydrothermal alteration in porphyry copper deposits. In: Pierce, F.W., Bohm, G.J. (Eds.), Porphyry copper deposits in American Cordillera. Ariz Geol Soci Dig, pp. 83–93.

Beane, R.E., Titley, S.R., 1981. Porphyry copper deposits. Part II. Hydrothermal alteration and mineralization. Econ Geol 75th Anniversary Vol, pp. 235–269.

Berberian, M., 1981. Active faulting and tectonics of Iran. In: Gupta HK, Delany FM, editors. Zagros-Hindu Kush-Himalaya geodynamic evolution. Am Geophys Union Geodyn Ser pp. 33–69.

Berberian, M., 1983. Continental deformation on the Iranian Plateau. Geological Survey of Iran: No. 52.

Berberian, F., Muir, I.D., Pankhurst, R.J., Berberian, M., 1982. Late Cretaceous and early Miocene Andean type plutonic activity in northern Makran and central Iran. J. Geol. Soc. Lond. 139, 605–614.

Bodnar, R.J., 1993. Revised equation and table for determining the freezing point depression of H_2O-NaCl solutions. Geochimica et Cosmochimica Actav. 57, 683–684.

Bodnar, R.J., 1995. Fluid inclusions evidence for a magmatic source for metals in porphyry copper deposits. In: Thompson, J.H. (Ed.), Magmatic fluids and ore deposits. Miner Associ Can Short Course, pp. 129–152.

Please cite this article as: Malekzadeh Shafaroudi, A., et al., The Khopik porphyry copper prospect, Lut Block, Eastern Iran: Geology, alteration and mineralization, fluid inclusion, and oxygen isotope studies, Ore Geol. Rev. (2014), http://dx.doi.org/10.1016/j.oregeorev.2014.04.015

Boomeri, M., Nakashima, K., Lentz, D.R., 2009. The Miduk porphyry Cu deposit, Kerman, Iran: a geochemical analysis of the potassic zone including halogen element systematics related to Cu mineralization processes. J. Geochem. Explor. 103, 17–29.

Brown, P.E., Lamb, W.M., 1989. P-V-T properties of fluids in the system H_2O-CO_2-NaCl: New graphical presentations and implications for fluid inclusion studies. Geochim. Cosmochim. Acta 53, 1209–1221.

Burnham, C.W., 1985. Energy release in subvolcanic environments: implications for breccia formation. Econ. Geol. 80, 1515–1522.

Burnham, C.W., Ohmoto, H., 1980. Late-stage processes of felsic magmatism. In: Ishihara, S., Takenouchi, S. (Eds.), Granitic magmatism and related mineralization. Mining Geology Special Issue. Society of Resources Geology of Japan, pp. 1–13.

Camp, V., Griffis, R., 1982. Character, genesis and tectonic setting of igneous rocks in the Sistan suture zone, eastern Iran. Lithos 15, 221–239.

Cline, J.S., 1995. Genesis of porphyry copper deposits: The behavior of water, chloride, and copper in crystalline melts. In: Pierce, F.W., Bohm, G.J. (Eds.), Porphyry copper deposits in American Cordillera. Ariz Geol Soci Dig, pp. 69–82.

Cloos, M., 2001. Bubbling magma chambers, cupolas, and porphyry copper deposits. Int. Geol. Rev. 43, 258–311.

Defant, M.J., Drummond, M.S., 1990. Derivation of some modern arc magmas by melting of young subducted lithosphere. Nature 347, 662–665.

Dilles, J.H., 1987. Petrology of the Yerington batholith, Nevada: Evidence for evolution of porphyry copper ore fluids. Econ. Geol. 82, 1750–1789.

Dilles, J.H., Einaudi, M.T., 1992. Wall-rock alteration and hydrothermal flow paths about the Ann-Mason porphyry copper deposit, Nevada- A6-km vertical reconstruction. Econ. Geol. 87, 1963–2001.

Dimitrijevic, M.D., 1973. Geology of the Kerman region. Geological Survey of Iran Report: No. 52.

Doglioni, C., Tonarini, S., Innocenti, F., 2009. Mantle wedge asymmetries and geochemical signatures along W- and E-NE directed subduction zones. Lithos 113, 179–189.

Eastoe, C.J., 1978. A fluid inclusion study of the Panguna porphyry copper deposit, Bougainville, Papua New Guinea. Econ. Geol. 73, 721–748.

Eftekharnejad, J., 1981. Tectonic division of Iran with respect to sedimentary basins. J. Iran. Pet. Soc. 82, 19–28 (in Persian with English abstract).

Esmaeily, D., Nedelec, A., Valizadeh, M.V., Moore, F., Cotton, J., 2005. Petrology of the Jurassic Shah-kuh granite (eastern Iran), with reference to tin mineralization. J. Asian Earth Sci. 25, 961–980.

Esperanca, S., Crisci, M., De Rosa, R., Mazzuli, R., 1992. The role of the crust in the magmatic evolution of the island Lipari (Aeolian Islands, Italy). Contrib. Mineral. Petrol. 112, 450–4620.

Forster, H., 1978. Mesozoic-Cenozoic metallogenesis in Iran. J. Geol. Soc. Lond. 135, 443–445.

Forster, H.J., Tischendorf, G., Trumbull, R.B., 1997. An evaluation of the Rb vs. (Y + Nb) discrimination diagram to infer tectonic setting of silicic igneous rocks. Lithos 40, 261–293.

Fournier, R.O., 1999. Hydrothermal processes related to movement of fluid from plastic into brittle rock in the magmatic-epithermal environment. Econ. Geol. 94, 1193–1211.

Frei, R., 1995. Evolution of mineralizing fluid in the porphyry copper system of the Skouries deposit, northeast Chalkidiki (Greece): Evidence from combined Pb-Sr and stable isotope data. Econ. Geol. 90, 746–762.

Geological Survey of Iran, 1975. Geological quadrangle map of Sar-e-Chah-e-Shur (1:100,000). Sheet No. 7754. Geological Survey of Iran.

Geological Survey of Iran, 1978. Geological quadrangle map of Mokhtaran (1:100,000). Sheet No. 7854. Geological Survey of Iran.

Ghasemi, A., Talbot, C.J., 2006. A new tectonic scenario for the Sanandaj-Sirjan zone (Iran). J. Asian Earth Sci. 26, 683–693.

Giggenbach, W.F., 1997. The origin and evolution of fluids in magmatic-hydrothermal systems, In: Barnes, H.L. (Ed.), Geochemistry of hydrothermal ore deposits, 3rd ed. John Wiley and Sons, New York, pp. 737–796.

Gokce, A., 2000. Ore deposits. Cumhuriyet University Publication.

Golonka, J., 2004. Plate tectonic evolution of the southern margin of Eurasia in the Mesozoic and Cenozoic. Tectonophysics 38, 235–273.

Gustafson, L.B.G., Hunt, J.P., 1975. The porphyry copper deposit at El Salvador: Chile. Econ. Geol. 70, 857–912.

Haghipour, A., Aghanabati, A., 1989. Geological map of Iran (1:2,500,000). Tehran. Geological Survey of Iran.

Hamoni, S.J., Karimpour, M.H., Malekzadeh Shafaroudi, A., Hajimirzajan, H., 2013. Geology, mineralization, geochemistry, and petrology of intrusive rocks in Rud-e-Gaz prospect area, southeast of Gonabad. Iran. J. Petrol. 4, 326–340 (in Persian with English abstract).

Harris, A.C., Golding, S.D., 2002. New evidence of magmatic-fluid-related phyllic alteration: Implications for the genesis of porphyry Cu deposits. Geology 30, 335–338.

Harris, A.C., Kamenetsky, V.S., White, N.C., Steele, D.A., 2004. Volatile phase separation in silicic magmas at Bajo de la Alumbrera porphyry Cu-Au deposit, NW Argentina. Resour. Geol. 54, 341–356.

Hass, J.L., 1971. The effect of salinity on the maximum thermal gradient of a hydrothermal system at hydrostatic pressure. Econ. Geol. 66, 940–946.

Hassanpour, S., 2010. Metallogeny and Mineralization of Cu-Au in Arasbaran Zone (NW Iran). (Ph.D. Thesis) University of Shahid Beheshti, Tehran p. 323 (in Persian).

Hedenquist, J.W., Richards, J.P., 1998. The influence of geochemical techniques on the development of genetic models for porphyry copper deposits. Rev. Econ. Geol. 10, 235–256.

Hedenquist, J.W., Arribas Jr., A., Reynolds, T.J., 1998. Evolution of an intrusion–centered hydrothermal system: Far Southeast–Lepanto porphyry and epithermal Cu–Au deposits, Philippines. Econ. Geol. 93, 373–404.

Heinrich, C.A., 2005. The physical and chemical evolution of low-salinity magmatic fluids at the porphyry to epithermal transition: A thermodynamic study. Miner. Deposita 39, 864–889.

Henley, R.W., McNabb, A., 1978. Magmatic vapor plumes and groundwater interaction in porphyry copper emplacement. Econ. Geol. 73, 1–20.

Hoefs, J., 1984. Stable isotope geochemistry, 3rd ed. Springer.

Hooper, R.J., Baron, I., Hatcher Jr., R.D., Agah, S., 1994. The development of the southern Tethyan margin in Iran after the break up of Gondwana: Implications of the Zagros hydrocarbon province. Middle East Pet. Geosci. 4, 72–85.

Hu, G.X., Clayton, R.N., 2003. Oxygen isotope salt effects at high pressure and high temperature and the calibration of oxygen isotope geothermometers. Geochim. Cosmochim. Acta 67, 3227–3246.

Hunt, J.P., 1991. Porphyry copper deposits. Econ. Geol. Monogr. 8, 192–206.

Jackson, J., McKenzie, D., 1984. Active tectonics of the Alpine-Himalayan belt between western Turkey and Pakistan. Geophys. J. R. Astron. Soc. 77, 185–264.

Jamali, H., Dilek, Y., Daliran, F., Yaghubpur, A.M., Mehrabi, B., 2010. Metallogeny and tectonic evolution of the Cenozoic Ahar-Arasbaran volcanic belt, northern Iran. Int. Geol. Rev. 52, 608–630.

Jankovic, S., 1984. Metallogeny of the Alpine granitoids in the Tethyan-Eurasian metallogenic belt. International Geological Congress, 27th: Moscow, pp. 247–274.

Jung, D., Kursten, M., Tarkian, M., 1976. Post-Mesozoic volcanism in Iran and its relation to the subduction of the Afro-Arabian under the Eurasian plate. In: Pilger, A., Rosler, A. (Eds.), A far between continental and oceanic rifting. Schweizerbartsche Verlagbuchhandlung Stuttgart, pp. 175–181.

Jung, D., Keller, J., Khorasani, R., Chr, Marcks, Baumann, A., Horn, P., 1983. Petrology of the Tertiary magmatic activity the northern Lut area, East of Iran. Geological Survey of Iran, Geodynamic Project (Geotraverse) in Iran: No. 51 pp. 285–336.

Karimpour, M.H., 2007. ASTER mineral mapping (20 scenes) to find target for mineral exploration in the Province of South Khorassan, Eastern Iran. Research & exploration report: South Khorasan Mines Department (in Persian).

Karimpour, M.H., Stern, C.R., 2010. Mineralogical and Chemical Composition of Tourmaline from Najmabad, Gheshlagh, Hired and Maherabad-Khopik, and their relationship with types of mineralization, Eastern Iran. Iran. J. Crystallogr. Miner. 18, 43–54.

Karimpour, M.H., Malekzadeh, Shafaroudi A., Hidarian Shahri, M.R., Askari, A., 2007. Mineralization, alteration, and geochemistry of Hired Au-Sn prospect area, South Khorasan province. Iran J Crystallger Miner 15, 67–90 (in Persian with English abstract).

Karimpour, M.H., Malekzadeh Shafaroudi A., Moradi, M., Farmer, L., Stern, C.R., 2013. Geology, mineralization, geochemistry, geochronology, and Rb/Sr and Sm/Nd isotopes of mineralization-related intrusive rocks of Kalath-Ahani area, south of Gonabad. Iran J Econ Geol 5, 267–290 (in Persian with English abstract).

Karimpour, M.H., Zaw, K., Huston, D.L., 2005. S-C-O isotopes, fluid inclusion microthermometry, and the genesis of ore bearing fluids at Qaleh-Zari Fe-oxide Cu-Au-Ag mine, Iran. Iran. J. Sci. 16, 153–169.

Karimpour, M.H., Malekzadeh Shafaroudi, A., Stern, C.R., Farmer, L., 2012. Petrogenesis of Granitoids, U-Pb zircon geochronology, Sr-Nd isotopic characteristic, and important occurrence of Tertiary mineralization within the Lut Block, eastern Iran. Iran. J. Econ. Geol. 4, 1–27 (in Persian with English abstract).

Kasemann, S., Meixner, A., Rocholl, A., Vennemann, T., Schmitt, A., Wiedenbeck, M., 2001. Boron and oxygen isotope composition of certified reference materials NIST SRM 610/612, and reference materials JB-2G and JR-2G. Geostand. Newslett. 25, 405–416.

Khashgerel, B.E., Rye, R.O., Hedenquist, J.W., Kavalieris, I., 2006. Geology and reconnaissance stable isotope study of the Oyu Tolgoi porphyry Cu-Au system, South Gobi, Mongolia. Econ. Geol. 101, 503–522.

Kirkham, R.V., Sinclair, W.D., 1988. Comb quartz layers in felsic intrusions and their relationship to porphyry deposits. In: Taylor, R.P., Strong, D.F. (Eds.), Recent advances in the geology of granite-related mineral deposits. Can Inst Min, pp. 50–71.

Kusakabe, M., Hori, M., Matsuhisa, Y., 1990. Primary mineralization-alteration of the El Teniente and Rio Blanco porphyry copper deposits, Chile: Stable isotopes, fluid inclusions and $Mg^{2+}/Fe^{2+}/Fe^{3+}$ ratios of hydrothermal biotite. Geology Department and University Extension, University of Western Australia Publication, Perth pp. 244–259.

Lecumberri-Sanchez, P., Steel-MacInnis, M., Bodnar, R.J., 2012. A numerical model to estimate trapping conditions of fluid inclusions that homogenize by halite disappearance. Geochim. Cosmochim. Acta 92, 14–22.

Lindenberg, H.G., Groler, K., Jacobshagen, V., Ibbeken, H., 1984. Post-Paleozoic stratigraphy, structure and orogenetic evolution of the southern Sabzevar zone and the Taknar block. Neues Jahrb. Mineral. Geol. Palaeontol. Abh. 168, 287–326.

Lotfi, M., 1982. Geological and geochemical investigation on the volcanogenic Cu-Pb-Zn-Sb ore mineralization in the Shurab-Gale chah and North West of Khur. (PhD Thesis) University of Hamburg, Persian (152 pp.).

Lowenstern, J.B., Sinclair, W.D., 1996. Exsolved magmatic fluid and its role in the formation of comb-layered quartz at the Cretaceous Logtung W-Mo deposit: Yukon Territory Canada. Trans. R. Soc. Edinb. Earth Sci. 87, 291–303.

Mahmoudi, S., Masoudi, F., Corfu, F., Megrabi, B., 2010. Magmatic and metamorphic history of the Deh-Salm metamorphic Complex, Eastern Lut Block, (Eastern Iran), from U-Pb geochronology. Int. J. Earth Sci. (Geol. Rundsch.) 99, 1153–1165.

Malekzadeh Shafaroudi, A., 2009. Geology, mineralization, alteration, geochemistry, microthermometry, radiogenic isotopes, petrogenesis of intrusive rocks and determination of source of mineralization in Maherabad and Khopik prospect areas, South Khorasan province. Unpublished PhD Thesis Ferdowsi University of Mashhad, Mashhad, Iran (536 pp. (in Persian)).

Malekzadeh Shafaroudi, A., Karimpour, M.H., 2013a. Hydrothermal alteration mapping in northern Khur, Iran, using ASTER image processing: a new insight to the type of copper mineralization in the area. Acta Geol. Sin. 87, 830–842.

Malekzadeh Shafaroudi, A., Karimpour, M.H., 2013b. Geology, mineralization, and fluid inclusion studies of the Howz-e-Rais lead-zinc-copper deposit, Eastern Iran. Iran. J. Adv. Appl. Geol. 6, 63–73 (in Persian with English abstract).

Malekzadeh Shafaroudi, A., Karimpour, M.H., Mazaheri, S.A., 2010. Rb-Sr and Sm-Nd isotopic compositions and petrogenesis of syn-mineralization intrusive rocks of

Please cite this article as: Malekzadeh Shafaroudi, A., et al., The Khopik porphyry copper prospect, Lut Block, Eastern Iran: Geology, alteration and mineralization, fluid inclusion, and oxygen isotope studies, Ore Geol. Rev. (2014), http://dx.doi.org/10.1016/j.oregeorev.2014.04.015

gold-rich porphyry copper Maherabad prospect area (north of Hanich), east of Iran. Iran. J. Crystallogr. Miner. 18, 15–32.

Malekzadeh Shafaroudi, A., Karimpour, M.H., Stern, C.R., 2012. Zircon U-Pb dating of Maherabad porphyry copper-gold prospect area: evidence for a late Eocene porphyry-related metallogenic epoch in east of Iran. Iran. J. Econ. Geol. 3, 41–60 (in Persian with English abstract).

Mehrabi, B., Talefazel, E., Nokhbatolfoghahai, A., 2011. Disseminated, veinlet, and vein Pb-Zn, Cu and Sb polymetallic mineralization in the Gale-Chah-Shurab mining district, Iranian East Magmatic Assemblage (IEMA). Iran. J. Econ. Geol. 3, 61–77 (In Persian with English abstract).

Middlemost, E.A.K., 1985. Magmas and magmatic rocks. Longman, New York.

Mirzaee, R., Ahmadi, A., Mirnejad, H., 2012. Mineralogy and fluid inclusion studies of Mahoor polymetallic deposit, east of Lut block, central Iran. Iran. J. Crystallogr. Miner. 20, 307–318 (in Persian with English abstract).

Mohajjel, M., Fergusson, C.L., Sahandi, M.R., 2003. Cretaceous-Tertiary convergence and continental collision, Sanandaj-Sirjan zone, western Iran. J. Asian Earth Sci. 21, 397–412.

Müller, D., Groves, D.I., 1993. Direct and indirect associations between potassic igneous rocks, shoshonites and gold-copper deposits. Ore Geol. Rev. 8, 383–406.

Nash, T.J., 1976. Fluid inclusion petrology data from porphyry copper deposits and applications to exploration. U.S. Geological Survey Professional Paper 907-D (16 pp.).

Norton, D.L., Cathles, L.M., 1973. Breccia pipes-Products of exsolved vapor from magmas. Econ. Geol. 68, 540–546.

Pearce, J.A., Harris, N.B.W., Tindle, A.G., 1984. Trace element discrimination diagrams for the tectonic interpretation of granitic rocks. J. Petrol. 25, 956–983.

Redmond, P.B., Einaudi, M.T., 2010. The Bingham Canyon porphyry Cu-Mo-Au deposit. I. Sequence of intrusions, vein formation, and sulfide deposition. Econ. Geol. 105, 43–68.

Richards, J.P., 2005. Cumulative factors in the generation of giant calc-alkaline porphyry Cu deposits. In: Porter, T.M. (Ed.), Super porphyry copper and gold deposits: A global perspective. PGC Publishing, Adelaide, pp. 7–25.

Richards, J.P., Spell, T., Rameh, E., Razique, A., Fletcher, T., 2012. High Sr/Y reflect arc maturity, high magmatic water content, and porphyry Cu ± Mo ± Au potential: examples from the Tethyan arcs of central and eastern Iran western Pakistan. Econ. Geol. 107, 295–332.

Roedder, E., 1984. Fluid inclusions. In: Ribbe, P.E. (Ed.), Reviews in Mineralogy, vol. 12. Mineral Soci Am (644 pp.).

Roedder, E., 1992. Fluid inclusion evidence for immiscibility in magmatic differentiation. Geochim. Cosmochim. Acta 56, 5–20.

Rumble, D., Hoering, T.C., 1994. Analysis of oxygen and sulfur isotope ratios in oxide and sulfide minerals by spot heating with a carbon dioxide laser in a fluorine atmosphere. Acc. Chem. Res. 27, 237–241.

Rusk, B.G., Reed, M.H., Dilles, J.H., Klemm, L.M., Heinrich, C.A., 2004. Compositions of magmatic hydrothermal fluids determined by LAICP-MS of fluid inclusions from the porphyry copper-molybdenum deposit at Butte, MT. Chem. Geol. 210, 173–199.

Saccani, E., Delavari, M., Beccaluva, L., Amini, S.A., 2010. Petrological and geochemical constraints on the origin of the Nehbandan ophiolitic complex (eastern Iran): implication for the evolution of the Sistan Ocean. Lithos 117, 209–228.

Samani, B., Ashtari, Sh., 1992. Geological evolution of Sistan and Baluchestan area. Iran. J. Geosci. 4, 72–85 (in Persian with English abstract).

Seedorff, E., Einaudi, M.T., 2004. Henderson porphyry molybdenum system, Colorado: I. Sequence and abundance of hydrothermal mineral assemblages, flow paths of evolving fluids, and evolutionary style. Econ. Geol. 99, 3–37.

Seedorff, E., Dilles, J.D., Proffett Jr., J.M., Einaudi, M.T., Zurcher, L., Stavast, W.J.A., Johnson, D.A., Barton, M.D., 2005. Porphyry deposits: characteristics and origin of hypogene features. Econ Geol 100th Anniversary Vol pp. 251–298.

Shafiei, B., Haschke, M., Shahabpour, J., 2009. Recycling of orogenic arc crust triggers porphyry Cu mineralization in Kerman Cenozoic arc rocks, southeastern Iran. Miner. Deposita 44, 265–283.

Shahabpour, J., 2007. Island-arc affinity of the Central Iranian Volcanic Belt. J. Asian Earth Sci. 30, 652–665.

Sharp, Z.D., 1990. A laser-based microanalytical method for the in determination of oxygen isotope ratios of silicates and oxides. Geochim. Cosmochim. Acta 54, 1353–1357.

Shepherd, T.J., Rankin, A.H., Alderton, D.H.M., 1985. A practical guide to fluid inclusion studies. Blackie, London.

Sheppard, S.M.F., 1986. Characterization and isotopic variations in natural waters. Rev. Mineral. 16, 165–183.

Sheppard, S.M.F., Nielsen, R.L., Taylor Jr., H.P., 1971. Hydrogen and oxygen isotope ratios in minerals from porphyry copper deposits. Econ. Geol. 66, 515–542.

Shinohara, H., 1994. Exsolution of immiscible vapor and liquid phases from a crystallizing silicate melt: Implications for chlorine and metal transport. Geochim. Cosmochim. Acta 58, 5215–5221.

Sillitoe, R.H., 2010. Porphyry copper systems. Econ. Geol. 105, 3–41.

Singer, D.A., Berger, V.I., Moring, B.C., 2008. Porphyry copper deposits of the world: Database and grade and tonnage models. U.S. Geological Survey Open File Report.

Skewes, M.A., Holmgren, C., Stern, C.R., 2003. The Donoso copper rich, tourmaline-bearing breccia pipe in central Chile: Petrologic, fluid inclusion and stable isotope evidence for an origin from magmatic fluids. Miner. Deposita 38, 2–21.

Steele-MacInnis, M., Lecumberri-Sanchez, P., Bodnar, R.J., 2012. HOKIEFLINCS-H2O-NACL: A Microsoft Excel spreadsheet for interpreting microthermometric data from fluid inclusions based on the PVTX properties of H_2O-NaCl. Comput. Geosci. 49, 334–337.

Stocklin, J., Nabavi, M.H., 1973. Tectonic map of Iran. Geological Survey of Iran.

Tarkian, M., Lotfi, M., Baumann, A., 1983. Tectonic, magmatism and the formation of mineral deposits in the central Lut, east Iran. Geological Survey of Iran, geodynamic project (geotraverse) in Iran: No. 51, pp. 357–383.

Taylor Jr., H.P., 1974. The application of oxygen and hydrogen isotope studies to problems of hydrothermal alteration and ore deposition. Econ. Geol. 69, 843–883.

Tirrul, R., Bell, I.R., Griffis, R.J., Camp, V.E., 1983. The Sistan suture zone of eastern Iran. Geol. Soc. Am. Bull. 94, 134–156.

Ulrich, T., Günther, D., Heinrich, C.A., 2001. The evolution of a porphyry Cu-Au deposit, based on LA-ICP-MS analysis of fluid inclusions: Bajo de la Alumbrera, Argentina. Econ. Geol. 96, 1743–1774.

Watanabe, Y., Hedenquist, J.W., 2001. Mineralogic and stable isotope zonation at the surface over the El Salvador porphyry copper deposit, Chile. Econ. Geol. 96, 1775–1797.

Waterman, G.C., Hamilton, R.L., 1975. The Sar-Cheshmeh porphyry copper deposit. Econ. Geol. 70, 568–576.

Webster, J.D., 1992. Fluid-melt interactions involving Cl-rich granites: Experimental study from 2 to 8 kbar. Geochim. Cosmochim. Acta 56, 659–678.

Williams-Jones, A.E., Heinrich, C.A., 2005. Vapor transport of metals and the formation of magmatic-hydrothermal ore deposits. Econ. Geol. 100, 1287–1312.

Zaraisky, G.P., Seltmann, R., Shatov, V.V., Aksyuk, A.M., Shapovalov Yu, B., Chevychelov, V. Y., 1997. Petrography and geochemistry of Li-F granites and pegmatite-aplite banded rocks from the Orlovka and Etyka tantalum deposits in Eastern Transbaikalia, Russia. In: Papunen (Ed.), Mineral deposits, pp. 695–698 (Rotterdam).

Zhang, L.G., Liu, J.X., Zhou, H.B., Chen, Z.S., 1989. Oxygen isotope fractionation in the quartz-water-salt system. Econ. Geol. 89, 1643–1650.

Zhang, Q., Wang, Y., Wang, Y.L., 2001. Preliminary study on the components of the lower crust in east China Plateau during Yangshanian Period: constraints on Sr and Nd isotopic compositions of adakite-like rocks. Acta Petrol. Sin. 17, 505–513 (in Chinese with English abstract).

Please cite this article as: Malekzadeh Shafaroudi, A., et al., The Khopik porphyry copper prospect, Lut Block, Eastern Iran: Geology, alteration and mineralization, fluid inclusion, and oxygen isotope studies, Ore Geol. Rev. (2014), http://dx.doi.org/10.1016/j.oregeorev.2014.04.015